OMI Algorithm Theoretical Basis Document

Volume I

OMI Instrument, Level 0-1b processor, Calibration & Operations

P.F. Levelt (Editor)
R. Noordhoek (Layout)

ATBD-OMI-01, Version 1.0, September 2001

Table of Contents

Preface

Preface to the four OMI-EOS Algorithm Theoretical Basis Documents (ATBDs) for the Ozone Monitoring Instrument (OMI), to be launched mid-2003 on NASA's EOS-Aura satellite

Background

OMI-EOS is a Dutch-Finnish ozone monitoring instrument that will fly on NASA's Aura Mission, part of the Earth Observation System (EOS). Since Aura's purpose is to carry out extensive studies of the Earth's atmosphere, OMI's measurements of ozone columns and profiles, aerosols, clouds, surface UV irradiance, and the trace gases NO_2, SO_2, HCHO, BrO, and OClO fit well into the Aura mission goals. A wide-swath, nadir-viewing, near UV-visible spectrograph, OMI draws heavily on European experience in the atmospheric research instruments GOME (on ERS-2), SCIAMACHY (to be launched later in 2001 on Envisat), and GOMOS (also onboard Envisat).

Purpose of the ATBD

This set of four OMI-EOS Algorithm Theoretical Basis Documents (ATBDs), is intended to present a detailed picture of the instrument and the retrieval algorithms used to derive atmospheric information from the instrument's measurements, so that there is a clear understanding of the results, within the community of OMI scientists, within the Aura Science Team, and among the atmospheric community at large. Each of the chapters of the four ATBDs is written by scientists responsible for the development of the algorithms presented.

These ATBDs will be presented to a group of expert reviewers recruited mainly from the atmospheric research community outside Aura. The results — critiques and recommendations — of the reviewers study of the ATBD will be presented at an Aura meeting, currently scheduled for 5 November 2001. Since changes to the instrument and the Level 0 to 1B processing have a potential for significant cost and schedule impact, the first ATBD is presented for purposes of comment and information. However, progression to the writing of acceptable, operational software for the algorithms for which the data products will be archived in the DAAC (Distributed Active Archive Centre) at NASA's EOSDIS in the other three ATBDs, depends on the approval of the ATBD by the Aura Mission Scientist.

Contents of the ATBDs

ATBD 1 contains a general description of the instrument and its measurement modes. In addition, there is a presentation of the Level 0 to 1B algorithms which convert instrument counts to calibrated radiances, ground and in-flight calibration, and the flight operations needed to collect science data. It is critical that this is well understood by the developers of the higher level processing, as they must know exactly what has been accounted for (and how), and what has not been considered in the Level 0 to 1B processing.

ATBD 2 covers the ozone products. Although OMI is nadir-viewing, this does not limit its output to vertical columns. Rather, because its output is a continuous, moderate-resolution spectrum that includes the range of ozone absorption, it is possible to develop an algorithm for vertical profile as well. The continuous spectrum also makes it possible to use a DOAS (Differential Optical Absorption Spectroscopy) technique developed in connection with GOME, flying on ERS-2. At the same time, an improved version of the TOMS total ozone column algorithm — developed and used successfully over 3 decades — will be used on OMI data. Rounding out the group of four algorithms in this ATBD is a separate, independent estimate of

tropospheric column ozone, using an improved version of the Tropospheric Ozone Residual (TOR) and cloud slicing methods developed for TOMS.

ATBD 3 presents retrieval algorithms for producing the aerosols, clouds, and surface UV radiation products. Retrieval of aerosol optical thickness and aerosol type is presented. Aerosols are of interest because they play an important role in tropospheric pollution and climate change.

The cloud products include cloud top height and effective cloud fraction, both of which are essential, for example, in retrieving the trace gas vertical columns accurately. Effective cloud fraction is obtained by comparing measured reflectance with the expected reflectance from a cloudless pixel and reflectance from a fully cloudy pixel with a Lambertian albedo of 0.8.

On the other hand, two complementary algorithms are presented for cloud-top height (or pressure). One uses a DOAS method, applied to the O_2–O_2 absorption band around 477 nm, while the other uses the filling-in of selected Fraunhofer lines in the range 352-398 nm due to rotational Raman scattering.

Surface UV irradiance is important because of its damaging effects on human health, and on terrestrial and aquatic ecosystems. OMI will extend the long, continuous record produced by TOMS.

ATBD 4 presents the retrieval algorithms for the “additional” trace gases that OMI will be able to monitor: NO_2, SO_2, HCHO, BrO, and OClO. These gases are of interest both because of their respective roles in atmospheric chemistry, as well as their potential for pollution. Extensive experience with GOME has produced spectral fitting techniques used in these newly developed retrieval algorithms, each adapted to the specific characteristics of OMI and the particular molecule in question.

Summary

Individually, the four OMI-EOS ATBDs present in detail how each of OMI’s data products are produced. Together they demonstrate the important contributions OMI makes to addressing Aura’s scientific questions.

P.F. Levelt (KNMI, The Netherlands) *Principal Investigato*r
G.H.J. van den Oord (KNMI, The Netherlands) *Deputy PI*
E. Hilsenrath (NASA/GSFC, USA) *Co-PI*
G.W Leppelmeier (FMI, Finland) *Co-PI*
P.K. Bhartia (NASA/GSFC, USA) *US ST Leader*

1. Introduction

P.F. Levelt[1]
[1]**Royal Netherlands Meteorological Institute (KNMI), De Bilt, The Netherlands**

The Ozone Monitoring Instrument (OMI) will be part of NASA's EOS-Aura satellite, which will be launched in mid-2003. The Aura spacecraft will circulate in a sun-synchronous polar orbit with a local afternoon equator crossing time at 13:45, providing global coverage in one day. The mission has a design lifetime of five years once in orbit. The Aura spacecraft contains four instruments. The Microwave Limb Sounder (MLS) and the High Resolution Dynamics Limb Sounder (HIRDLS) are limb sounding instruments. The Ozone Monitoring Instrument (OMI) is a nadir sounder, and the Tropospheric Emission Spectrometer (TES) has both limb sounding and nadir sounding modes. MLS is on the front of the spacecraft while HIRDLS, TES and OMI are mounted on the nadir side. These locations were chosen so that the instruments could sample the same air mass within minutes.

Aura's specific mission objectives are to observe the atmosphere in order to answer the following three high priority environmental questions [*RD-1, RD-2*]:

1. Is the Earth's ozone layer recovering?
2. Is air quality changing? and
3. How is the Earth's climate changing?

The science goals of OMI are directly related to these questions and focus on (1) measuring the ozone layer and its destroying trace gases BrO and OClO, (2) tropospheric pollution by ozone, nitrogen dioxide, tropospheric aerosols, SO_2 and formaldehyde, and (3) detection of species important for climate change like aerosols, clouds and ozone.

The OMI instrument is a nadir looking instrument which measures the radiation backscattered by the Earth's atmosphere and surface over the entire wavelength range from 270 to 500 nm, with a spectral resolution of about 0.5 nm. The heritage of OMI are the European ESA instruments GOME and SCIAMACHY, which introduced the concept of measuring the complete spectrum in the ultraviolet/visible/near-infrared wavelength range with a high spectral resolution. This enables one to retrieve several trace gases from the same spectral measurement. The American predecessor of OMI is NASA's TOMS instrument. TOMS uses only 8 wavelength bands, from which the ozone column can be obtained very accurately. TOMS has the advantage that it has a fairly small ground-pixel size (50×50 km^2) in combination with a daily global coverage. OMI combines the advantage of GOME and SCIAMACHY with the advantage of TOMS, measuring the complete spectrum in the ultraviolet/visible wavelength range with a very high spatial resolution (13×24 km^2) and daily global coverage. This is possible by using a two-dimensional detector, as has been used e.g. in the GOMOS and MERIS satellite instruments in comparable wavelength ranges. The small pixel sizes enables OMI to look "in between" the clouds, which is very important for retrieving tropospheric information.

The purpose of this ATBD is to give the reader insight in the technical design of OMI and the level 0 to 1B processor, without discussing every technical detail, but in such a way that the reader can use the level 1B data for development of their level 1B to 2 algorithms. For more

detailed information the reader is directed to the relevant documents, which are mentioned in the text.

Since the performance and calibration measurements of the flight model of OMI have not been done yet, the expected performance of the instrument which are mentioned in this ATBD are taken from the Science Requirements Document (SRD) [*RD-3*].

1.1. References

RD-1 1999 EOS Reference Handbook, NASA, King, M.D. and R. Greenstone (eds.)
RD-2 EOS AURA website, http://eos-aura.gsfc.nasa.gov/
RD-3 Science Requirements Document for OMI-EOS, RS-OMIE-KNMI-001, Version 2, December 2000. ISBN 90-369-2187-2, KNMI publication: 193

2. Instrument Description

P.F. Levelt[1], J.P. Veefkind[1], R.H.M. Voors[1] and J. de Vries[2]
[1]Royal Netherlands Meteorological Institute (KNMI), De Bilt, The Netherlands
[2]Fokker Space, Leiden, The Netherlands

The Ozone Monitoring Instrument (OMI) is a nadir pointing spaceborne imaging spectrograph. It measures the reflected solar radiation in the ultraviolet and visible part in the spectral range that is between 270 and 500 nm, using two channels with a spectral resolution of about 0.5 nm (see Table 2.1). The nadir pointing telescope of OMI has a very large field of view of 114°, which is used for swath registration, perpendicular to the flight direction of the satellite. Due to this wide field of view of 114°, the OMI swath width is 2600 km, which provides daily global coverage.

Each of the two optical channels has a two dimensional detector (CCD). One dimension of the CCD is used to cover the spectrum, the other direction is used to cover the viewing direction rows, as illustrated in Figure 2.1. The UV channel consists of two sub-channels with the following full performance ranges: the UV-1, ranging from 270 to 310 nm, and the UV-2 ranging from 310 to 365 nm. The spectral and spatial sampling of the UV-1 are reduced by a factor of two compared to the UV-2. The full performance range of the VIS-channel ranges from 365 to 500 nm. The spectral sampling distances and resolutions can be found in Table 2.1.

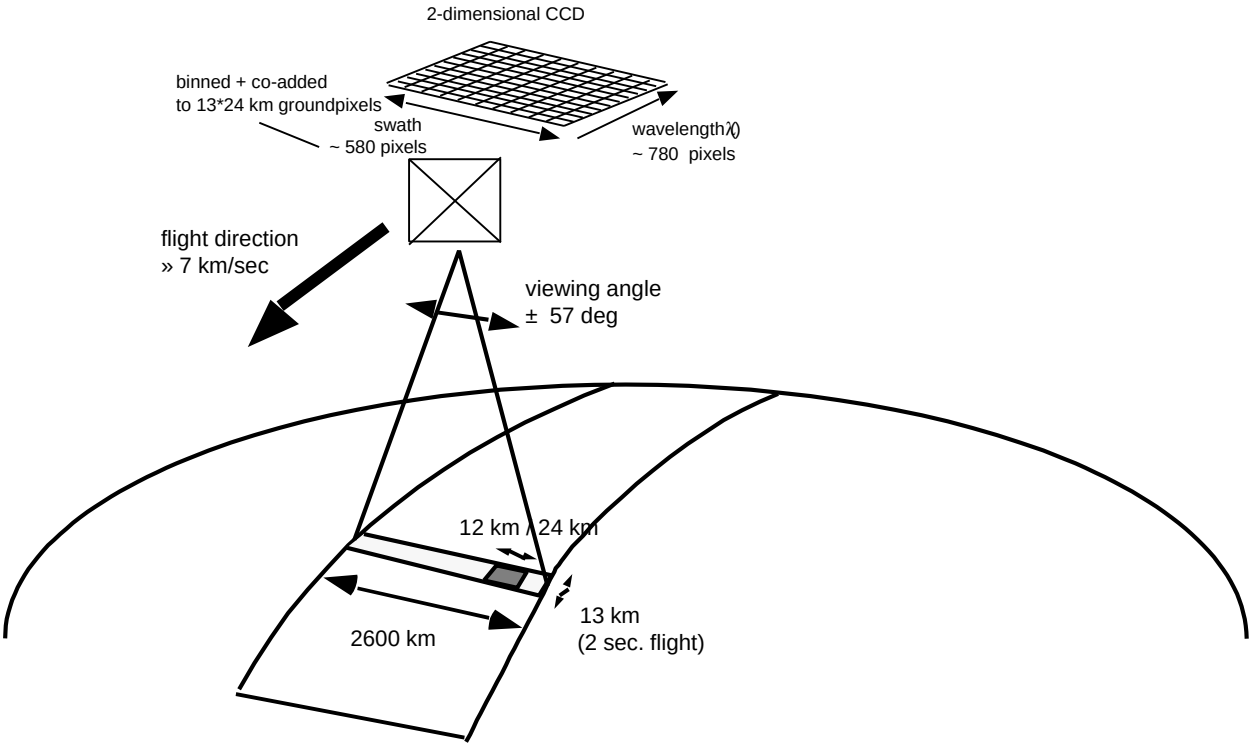

Figure 2.1 Measurement principle of OMI. *Courtesy of Fokker Space*

The main observation modes for OMI are the Global measurement mode, the Spatial zoom-in measurement mode and the Spectral zoom-in measurement mode. The Global Measurement mode is the default mode and samples the complete swath of 2600 km for the

complete wavelength range. The ground pixel size at nadir position in the Global mode is 13 × 24 km^2 (along × across track) for the UV-2 and VIS channels, and 13 × 48 km^2 for the UV-1 channel.

Table 2.1 Spectral performance range, resolution and sampling distances and spectral resolutions

Channel	Full performance range	Average Spectral resolution (FWHM)	Average Spectral sampling distance
UV-1	270 - 310 nm	0.42 nm	0.32 nm/pixel
UV-2	310 - 365 nm	0.45 nm	0.15 nm/pixel
VIS	365 - 500 nm	0.63 nm	0.21 nm/pixel

In the Spectral and Spatial zoom-in modes the ground pixel size is reduced to 13 × 12 km^2 for the UV-2 and VIS, and 13 × 24 km^2 for the UV-1. Hence, in the zoom-in modes the ground pixel size in the across track direction is reduced by a factor of two. In the Spatial zoom-in mode the complete wavelength range is available, but for the UV-2 and VIS channels the swath is reduced to 725 km. For the UV-1 the complete swath is available. In the Spectral zoom-in mode the complete swath is available, but the wavelength range is limited to 306-432 nm. Thus, in Spectral zoom-in mode the UV-1 is not available, and only the shorter wavelengths of the VIS channel are available.

The pixel-size in the swath-direction increases from 13 × 24 km^2 (exact nadir position) to 13 × ~128 km^2 at the most outer swath-angle (57 degrees). This effect is illustrated in Figure 2.2.

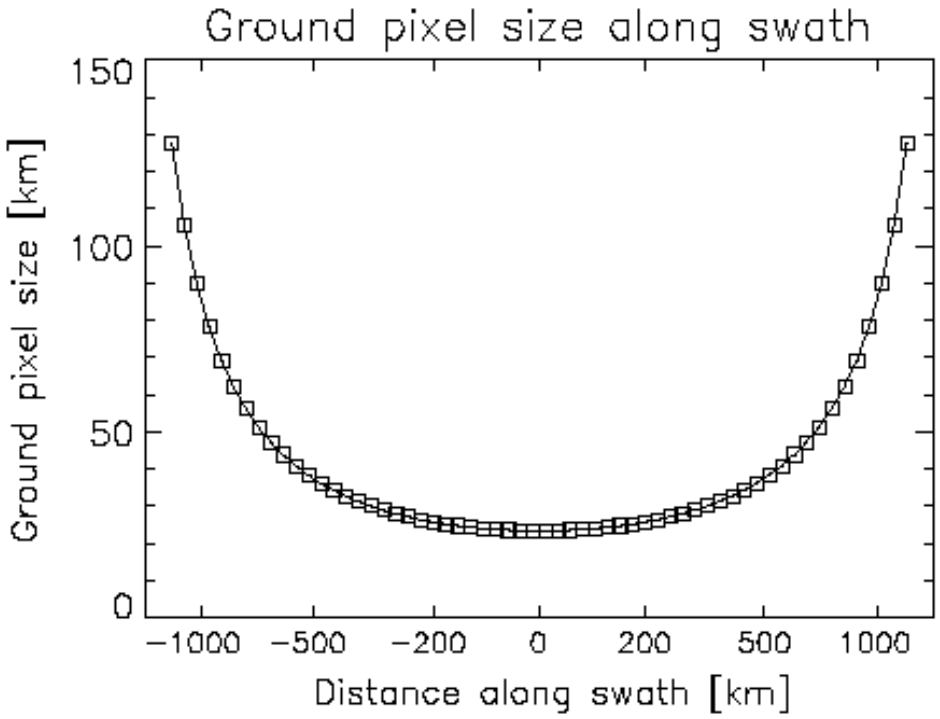

Figure 2.2 Ground pixel size in swath direction as a function of the ground pixel number.

In addition to the nominal operational mode, OMI will also perform in-flight calibration measurements. The most important in-flight calibration measurement is the observation of the Sun. Once per orbit the Sun irradiates the solar calibration port which makes it possible to observe the Sun by opening the Sun aperture and rotating a folding mirror and a diffuser in the

light path. Three diffusers are available for solar measurements. One is intended for daily use, whereas the others are used to monitor the degradation of the daily used diffuser. To monitor the overall performance of the instrument, OMI has an internal White Light Source (WLS). The WLS is observed via a transmission diffuser. To separately check the sensitivity of the CCD pixels, there are also Light Emitting Diodes (LEDs) available.

2.1. General description of the instrument

Figure 2.3 shows the conceptual design of the OMI with the large field-of-view out of the plane of the paper. The OMI instrument is composed of the following three elements:

4. Optical Assembly (OA), consisting of the Optical Bench (OPB), two Detector Modules (DEM), and Thermal Hardware
5. Electronics Unit (ELU), performing CCD readout control and analogue-to-digital conversion
6. Interface Adaptor Module (IAM), performing Command Buffering as well as the Data Formatting and Satellite Bus Interface functions.

In sections 2.2, 2.3 and 2.4 the Optical Assembly (OA), the Electronic Unit (ELU) and Interface Adaptor Module (IAM) are each described in more detail, respectively.

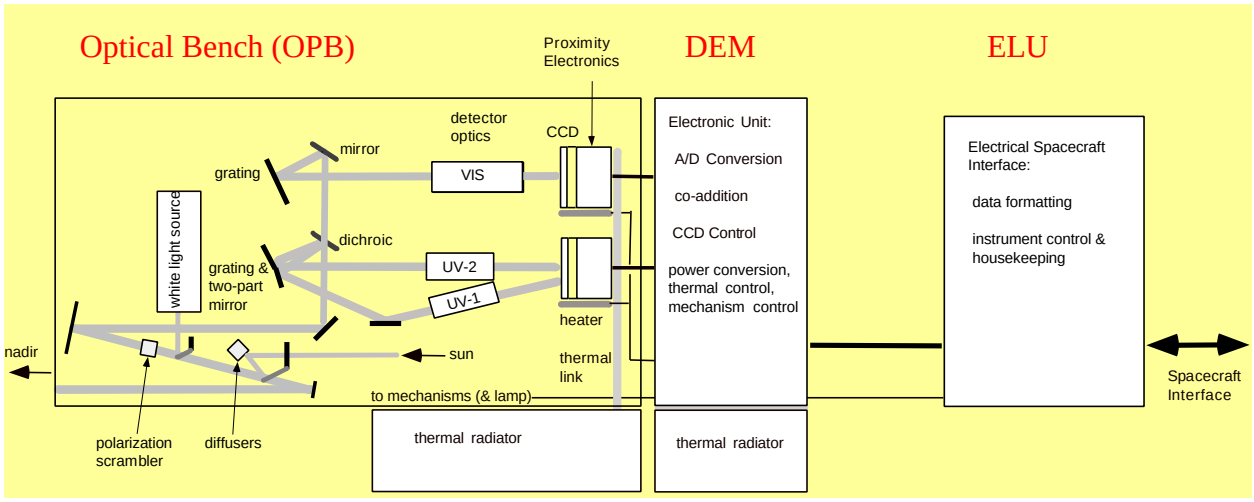

Figure 2.3 Conceptual design of the OMI *Courtesy of Fokker Space*

2.2. Optical Assembly

In the Optical Assembly the radiance and irradiance is collected and split according to wavelength and focussed on the detector modules of the two channels. The Optical Bench consists of a single aluminium structure in which all elements are mounted. Attached to this aluminium structure are the two Detector Modules. The Optical Assembly Thermal Hardware consists of a thermal radiator and heaters. The thermal radiator is thermally connected to the detector modules via a cold-finger and a flex-link. The heaters are attached to the Optical Bench structure and the CCD detectors.

The Optical Bench, Detector Modules, and Optical Assembly Thermal Hardware are described in more detail in sections 2.2.1 and 2.2.2.

2.2.1. Optical Bench

The OPB consists of a telescope, UV channel, visible channel and calibration systems. For switching between Earth observations and the different calibration modes, the Optical Bench uses three mechanisms (see “Mechanisms”). In Figure 2.4 the optical layout of the telescope, UV-1 and UV-2 channel and the calibration optics are shown.

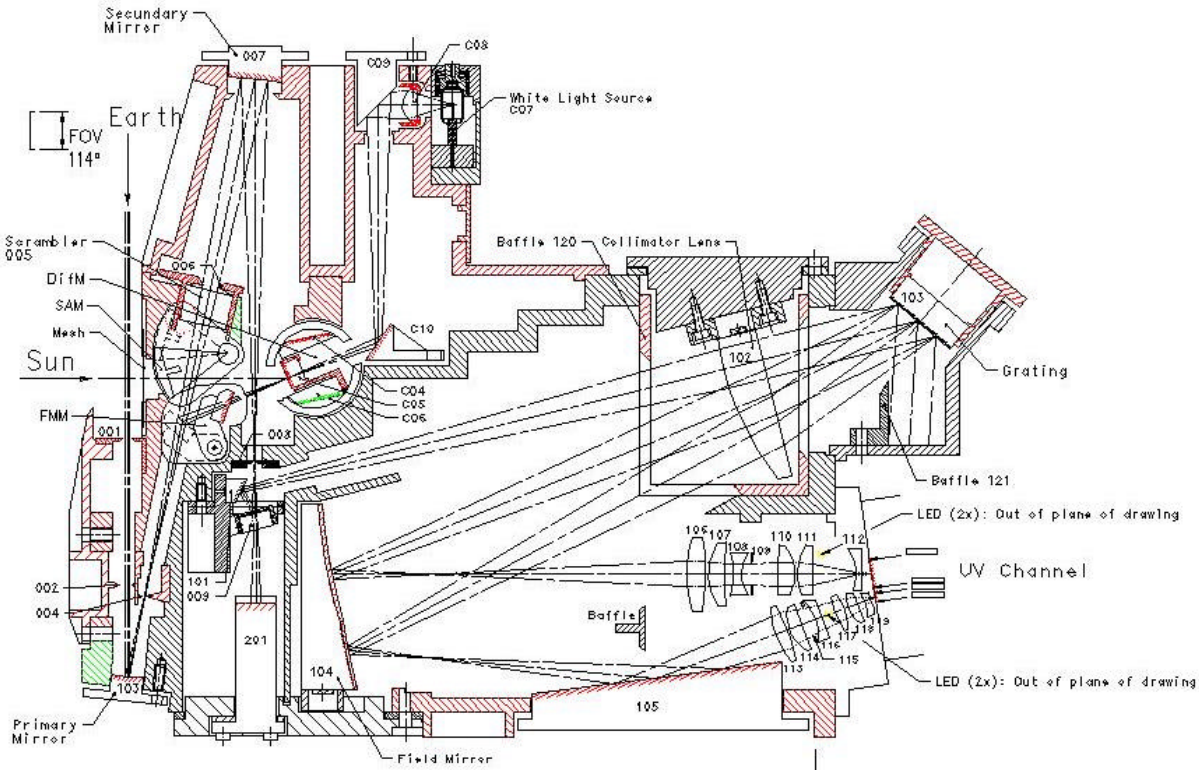

Figure 2.4 Optical layout of the telescope, UV-1 and UV-2 channel and the calibration optics Ó Fokker Space

Telescope

The telescope is a wide field reflective telecentric configuration. The telescope consists of two spherical mirrors (103 and 007). Radiation from the Earth is imaged on the entrance slit (008) of the spectrometer. Between the primary and secondary mirror a polarisation scrambler (005) is positioned close to the aperture stop (006) of the telescope. The large FOV 114° is in the plane perpendicular to the plane of drawing. The secondary mirror has a coating to suppress straylight from 500 nm up towards longer wavelengths.

Scrambler

The OMI spectrometer is sensitive to the polarisation of the incoming radiation (due to polarisation dependent properties of mirrors, dichroics and gratings). Therefore, Earth radiances with exactly the same intensity but a different polarisation will give a different detector signal. The purpose of the polarisation scrambler is to make the instrument insensitive to the polarisation of the received radiation.

In principle a scrambler transforms one polarisation state into a continuum of polarisation states and thus not into totally unpolarized light. Therefore a scrambler is called a pseudo-depolariser. For OMI-EOS a spatial pseudo-polarises is applied, which transforms the input into an output of which the polarisation state varies with position over the scrambler exit aperture. Polarisation effects due to the primary mirror are compensated for by the first scrambler surface.

UV channel

Behind the entrance slit (008) a dichroic mirror (009) reflects the spectral range of the UV channels to folding mirror (101) and transmits the VIS spectral range to a flat mirror (201), that reflects the light at 90 degrees out of the plane of drawing.

The UV radiation is reflected by mirror (101) to a plano convex fused silica lens (102), that collimates the beam from the entrance slit in the direction of the grating (103). The function of the collimating / imaging lens (102) is twofold: it creates a parallel incoming beam on the grating (103) and forms an intermediate spectrum of the diffracted beams close to the field mirror (104). The grating (103) is used in the first order.

The layout of the UV channel is determined to a large extent by the straylight requirements especially for the UV-1 spectral area (270 - 310 nm). Within the UV spectral range the variation in radiance from the Earth between the shortest wavelength ($\lambda < 290$ nm) and the longer wavelength ($\lambda > 320$ nm) varies by more than three orders of magnitude. Without proper action the straylight at wavelengths below 290 nm exceeds the signal itself. This straylight originates from wavelengths between 310 to 380 nm. To avoid this unwanted situation, the UV channel is split into to sub-channels: UV-1 and UV-2.

An intermediate UV spectrum is created, close to a (split) field mirror (104). This field mirror is supplied with a coating with a wavelength (= position) dependent variable reflection in order to suppress the straylight of larger wavelengths in the extreme UV. Depending on the bandwidth of reflection coating (at each position), a suppression of straylight of one order of magnitude is reached.

Moreover by splitting the spectral range in 2 parts, the straylight that is caused by internal reflections in the UV-2 imaging objective, has no effect on the UV-1 spectrum at the detector surface.

The UV-1 image is scaled down by a factor of 2 on the CCD compared to the UV-2 image, in order to improve the S/N performance of the UV-1 channel by a factor of $\sqrt{2}$, at the cost of doubling the groundpixel size in the swath direction.

VIS channel

In Figure 2.5 the optical layout of the visible channel is shown. Note that the orientation of the plane of drawing of Figure 2.5 is perpendicular to that of Figure 2.4. The “visible” part of the spectrum (350 - 500 nm) is reflected by mirror (201) via folding mirror (202) to a collimating mirror (203). The rest of the visible channel is rather straight forward and consists of 2 folding mirrors (204 and 206), a plane grating with 1350 gr/mm (207) and an objective (209 - 213) to image the diffracted beams on the second detector.

Calibration Devices

OMI has the following on-board calibration/characterisation devices: A White Light Source (WLS) and Light Emitting Diodes (LEDs). The white light source (C07 in Figure 1.1) is a Tungsten Halogen lamp with a quartz bulb.

The main purpose of the WLS is pixel-to-pixel calibration where every pixel is illuminated by the proper wavelength (see also chapter 4).

Two LED’s, emitting at 570 nm, are positioned very close to the CCD-detector. The position of the green LED’s in the VIS channel is at the aperture 208 (see Figure 2.5). In the UV channels two LED’s are placed between lenses (110) and (111) (UV2) and two LED’s are placed between lenses (116) and (117) (see Figure 2.4).

The primary use of the LED’s is identification of bad pixels and to obtain the relative electronic gain values (see also chapter 4).

Finally it should be mentioned that the readout of the read-out register after a draindump (which accompanies every image) can be used to determine the readout noise and the electronic offset values.

The WLS will be operated once per week. The LED's will be operated once per day.

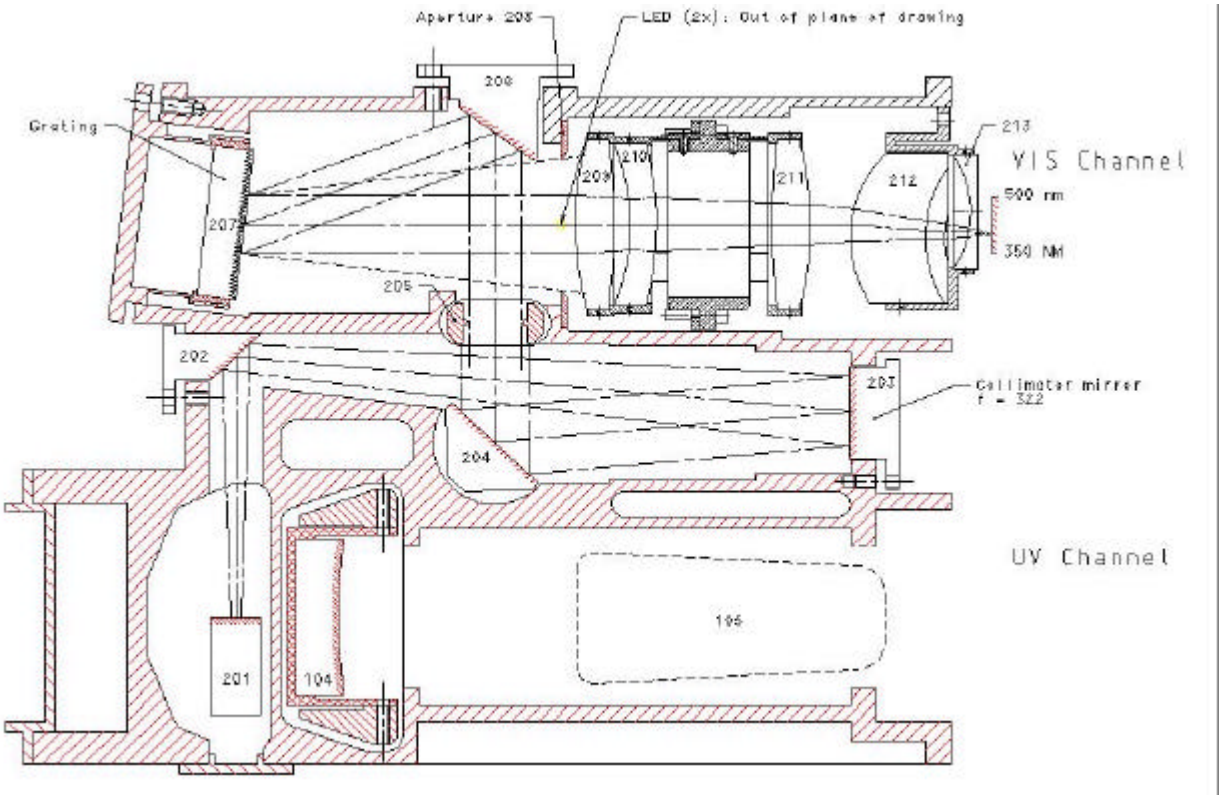

Figure 2.5 Optical layout of the visible channel *Courtesy of Fokker Space*

Mechanisms

In the OPB the following mechanisms can be identified:

- The Diffuser Mechanism (DifM). The diffusers play a key role in providing the sun-normalised spectrum, during the on-ground calibration the diffusers are therefore extensively calibrated. This mechanism contains one quartz transmission diffuser for the WLS calibration and two surface reflectance aluminium diffusers and one reflectance quartz plate volume diffuser for the solar calibration measurement. The transmission diffuser is to provide homogeneous illumination of the spectrograph slit during a WLS measurement. The reflectance quartz plate volume diffuser is used on a daily basis to provide the irradiance spectrum for normalising the earth radiance spectra. One surface reflectance aluminium diffuser will be used on a weekly basis for regular radiometric calibration verification, while the other will be used on a monthly basis as a backup in order to monitor the spectral degradation of the weekly aluminium diffuser. Irradiance measurements via the aluminium diffusers provide absolute radiometric irradiance calibration information. The quartz plate volume diffuser exhibits smaller spectral diffuser surface interference features compared to the aluminium surface reflectance diffusers, which makes it most suitable for normalising the earth radiance spectra, but it

too can be used for radiometric calibration purposes as well. All on-board diffusers are optimally protected from optical degradation by exposure to space environment.

- The Folding Mirror Mechanism (FMM), which contains a mirror, is used during Sun and WLS calibration and is positioned in the optical path of the telescope between the primary and secondary mirror to image the light of the diffusers on the spectrograph entrance slit.

- The Sun Aperture Mechanism (SAM), allows sunlight to enter the instrument for the solar calibration measurement. The SAM is a shutter that is always closed, except during the solar calibration measurements. In the aperture of the instrument behind the shutter, a mesh is mounted in order to reduce the intensity of the solar radiation. Keeping the shutter closed also prevents space debris and stray-light to enter the OPB.

Optical Path of Earth, solar, WLS and LED measurements.

The optical paths for the Earth and solar measurements are not the same. Therefore the optical paths could degrade differently during the mission which may produce an artificial trend in the Earth radiance to solar irradiance ratio. The on-board light sources will help diagnose this problem as will be discussed in chapter 4. The value of the on-board light source measurements is however also limited by their specific optical paths.

For an Earth measurement the complete optical path of the radiation is shown in Figure 2.4 for the UV-channel and in Figure 2.5 for the VIS channel. The radiation enters the instrument by aperture (001), reflects from the primary mirror (103), passes the scrambler (005) and reflects from the secondary mirror (007) before entering the spectrometer by entrance slit (008). Directly after the entrance slit the radiation is split by a dichroic mirror (009) reflecting the light into the UV-channel and passing the light to the VIS-channel.

For a solar calibration measurement, the SAM is opened so that the radiation of the sun can enter the instrument. This sunlight is then reflected by one of the three reflection diffusers (DifM mechanism) towards the FMM mirror, which has been moved in the optical path of the telescope, in order to reflect the solar radiation via the scrambler (005) towards the secondary mirror (007). A solar calibration measurement has therefore a different optical path from the Earth radiation measurement, adding the mesh, the reflection diffuser and the FMM mirror, and missing the primary mirror (103). The philosophy is that the FMM and the primary mirror, being made of the same material, will have a comparable degradation.

During a WLS measurement the transmission diffuser (C05) is used (DifM mechanism) and the Folding Mirror FMM is moved again into the optical path of the telescope. The WLS-radiation, passes lens (C08), reflects from mirrors (C09) and (C10), passes the transmission diffuser and reflects by the FMM via the scrambler (005) towards the secondary mirror (007). Therefore also in the case of the WLS measurements, several optical elements are added to the light-path and the same optical elements are removed as in the case of the solar calibration measurement. With the WLS most of the optical path can however be checked on degradation.

The LEDs are in front of the CCD detectors with only a few optical elements in between.

2.2.2. Detector Modules

The main function of the (DEM) is to convert the optical signal provided by OPB, to an analogue electrical signal. The OMI-EOS system includes two identical DEMs. Each DEM consists of a CCD, control electronics and thermal hardware.

CCDs

Each OMI-EOS CCD is a thinned, back side illuminated CCD with a HfO_2 anti-reflection coating to realise a high quantum efficiency especially in the UV. This coating is optimised to have minimum reflectivity and best quantum efficiency at 270 nm.

The OMI detectors are so-called frame transfer CCD's. This means that the CCD's have three sections: an image section, a storage section, and a read-out register, as illustrated in Figure 2.6. The pixels are 22.5×22.5 micron in size and there are no regions in between the pixels that are not sensitive to light, which is important for accurately detecting spectral features of trace gases. Each image part of the CCD consists of 580×780 CCD pixels, of which 480×750 are used for the Earth measurements. The storage region of the CCD is an exact copy of the image part of the CCD. The read-out register has 17 extra pixels on each end.

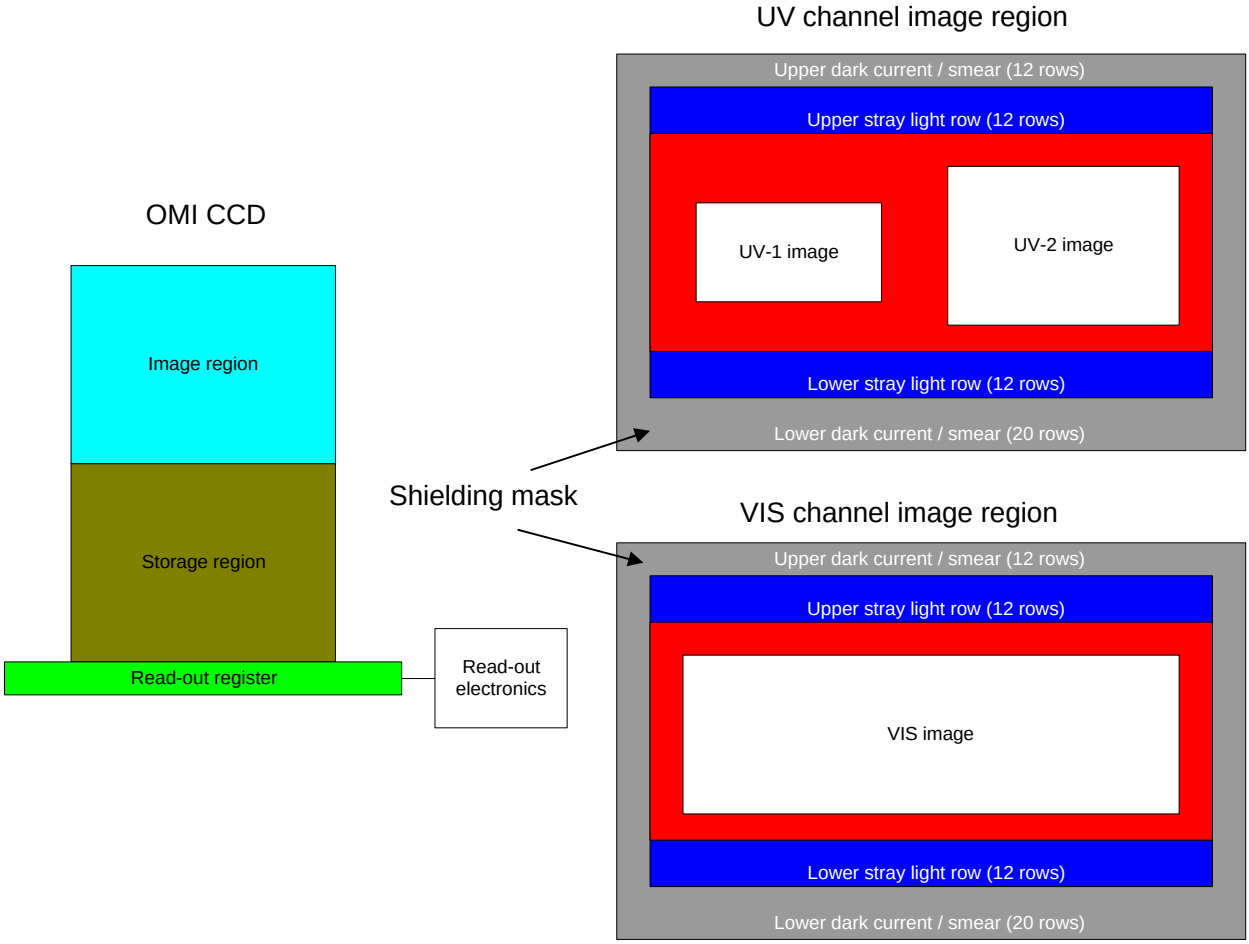

Figure 2.6 CCD detector layout *Courtesy of Fokker Space*

The CCD uses 480 rows of 750 pixels for the Earth measurements. The wavelength information is distributed along a CCD row, the spatial information is distributed along a CCD column. The image section is in the focal plane of the spectrograph (blue area in the left panel of Figure 2.6), and after exposure the signal for each pixel is transferred rapidly to the storage region (dark-green/brown area in the left panel Figure 2.6); this is called a 'frame transfer'. During transfer illumination of the detector continues, causing smearing of the signal. This so-called "smear"effect will be corrected for in the Level 0 to 1B software (see chapter 3). After transfer to the storage region, the rows are transfered to the read-out register (light-green area in

Figure 2.6) after which every read-out register pixel is separately evaluated. This process is called “clocking out”. Thus, the complete exposure time is available for read-out and the read-out process itself maintains the continuity of the measurements.

In Figure 2.7 the clock-out sequence of the CCD is schematically represented. In the first picture in Figure 2.7 the frame-transfer is shown. In the second picture it is shown that the rows of the storage area are clocked to the read-out register. In this process, 4 or 8 rows are added in the read-out register, before clocking them out over the read-out amplifier. This process is called ‘binning’ and is needed to reduce the data-rate for the read-out process of the CCD. Binning of 4 rows results in the zoom-in mode pixel size of 13×12 km^2, binning of 8 rows in the global mode pixel size of 13×24 km^2. For the UV-1 this ground-pixels sizes are respectively 13×24 km^2 and 13×48 km^2. The third picture shows the read-out process, where every binned row in the read-out register is clocked out to the right over an electronic amplifier.

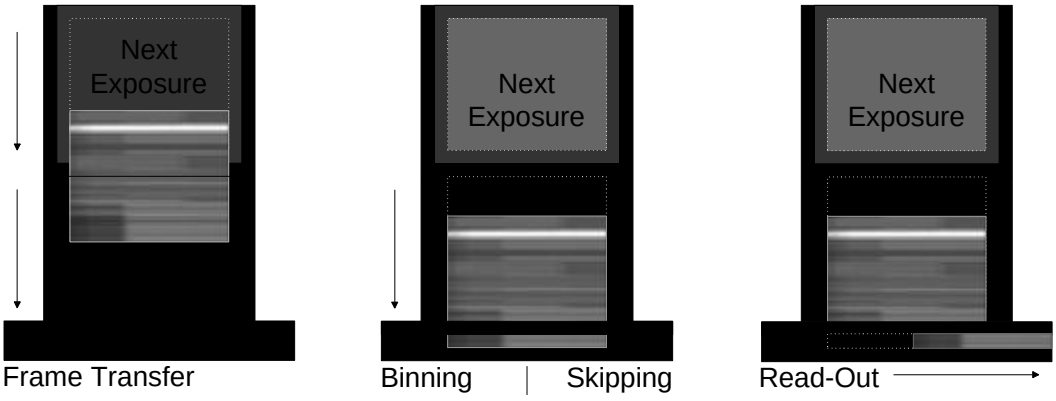

Figure 2.7 CCD Read out sequence *Courtesy of Patria Finavitec*

The nominal exposure time of the CCD is 0.4 seconds which is a carefully estimated balance between having enough signal in the UV-1 and preventing saturation in the VIS channel under most atmospheric conditions. In order to improve on S/N and to reduce the down link data-rate even more, 5 sequentially taken exposures are co-added. Co-adding is done by the electronics in the ELU. Co-addition of 5 exposures results in a 2 seconds interval in which measurements are taken in the flight-direction. This results in the 13 km spatial resolution in the flight direction. This 2 seconds interval is defined as being the ‘master clock period’ which is the time-interval that rules the ELU.

The right panels of Figure 2.6 show the layout of the image region for the UV and VIS channel. The extreme rows and columns of the image area (grey areas in Figure 2.6) are covered and not sensitive to light. These are used as a measure for dark signal (columns) and exposure smear (rows).

The image with measurement data does not cover the complete CCD image area and the remaining area contains stray light information. This concerns several rows above and below the image in the UV-2 and visible channel and somewhat more around the UV-1 channel. These areas are shown in blue in Figure 2.6. The rows above and below the image are again binned to achieve the best signal-to-noise.

Information on the electronics offset and dark current can also be obtained from the read-out register. The read-out register within the CCD (green area in Figure 2.6) has an excess of 17 pixels compared to the CCD itself. The offset can be measured via initial register readout

preceding all image data. As the register is cleared just before this, it also contains the offset data (this is called draindump).

The detector electronics consists of a 12 bit ADC, which allows for switching the gain as a function of the column number or wavelength to optimise signal to noise ratios. Switching as a function of wavelength results in more gain and therefore low noise for low radiance levels and improves the signal-to-noise ratio in the extreme UV. OMI allows for selection of the highest gain for the dark current / smear rows and stray light rows above and below the measurement data. The register readout uses the same gain switching as the image area ensuring that offset values for all gains are obtained. OMI allows to select four gain values.

Due to radiation damaging, the dark current of the CCDs will increase over the lifetime of OMI. To maintain low dark current towards the end of the mission, the nominal detector operating temperature is about –10 ºC. However, to avoid the risk of ice-formation on the surface of the detectors, outgassing of the instrument will take place as soon as possible after launch. A considerable amount of shielding is added to minimise detector degradation.

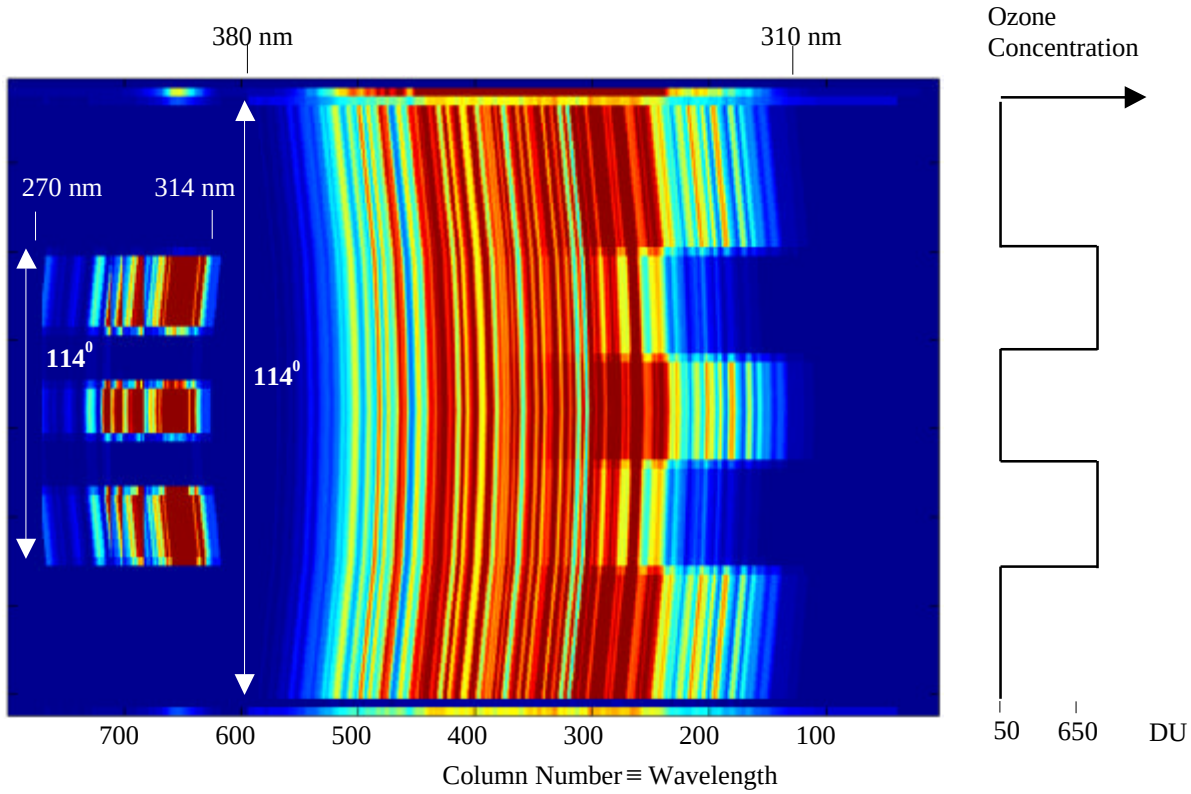

Figure 2.8 *Example OMI focal plane image.* *Courtesy of Fokker Space*
The columns represent the wavelength scale, the rows the viewing angle scale. The image shows the UV-1 channel data on the left and the UV-2 data on the right. The rows show two spectra distributed over 5 horizontal bands; one of the spectra represents an ozone total column of 50 and the other of 650 DU. The figure also shows the stray light and dark/smear rows binned into one row.

The optics of the instrument introduces some optical distortion of the image that is focused on the CCD. This is shown in Figure 2.8. The optical distortion has two components. Firstly, optical distortion in the swath direction (i.e. curvature of lines of equal viewing direction). Secondly, optical distortion in the spectral direction (i.e. curvature of lines of equal wavelength). The optical distortion in the swath direction introduces spatial aliasing: pixels which are part of the same row (i.e. pixels which are part of the same spectrum) having different viewing angles. Due to binning of the rows in the read-out register the optical distortion in the

spectral direction could introduces a decrease in the spectral resolution. This has however a negligible effect on the spectral resolution. Therefore the design is optimised to minimise to the distortion in the spatial direction. In the figure, this distortion is therefore hardly visible. The optical distortion in the spectral direction is clearly visible.

With the help of ray tracing programs the distortions have been calculated. Table 2.2 shows the maximum distortions in both spectral and swath direction for the channels. Note that the pixel size of the CCD is $22.5 \times 22.5\ \mu m^2$.

Table 2.2 Optical distortions of the channels [RD-1]

Channel	Maximum distortion in Spectral direction	Maximum distortion in Swath direction
UV-1	0.2 mm (~9 pixels)	< 4 μm (~0.2 pixel)
UV-2	0.38 mm (~ 17 pixels)	< 5 μm (~0.25 pixel)
Visible	0.05 mm (~2 pixels)	< 7 μm (~0.3 pixel)

Small Pixel Data

Per CCD one specific wavelength can be chosen for which no co-addition takes place, giving 5 separate points in the flight direction in stead of one. The exposure time is then 0.4 seconds in stead of 2 seconds, resulting in a sampling of 2.6 km in the flight direction. Because OMI's instantaneous field-of-view in the flight direction is about 10 km, these small pixel data are partly overlapping. In the swath direction these pixels are the same as for the global mode (24 km) and the zoom-in modes (12 km). This wavelength is programmable and can be optimised during flight. These small pixel data will be used in order to get sub-pixel information on cloud-fraction.

Control electronics

The control electronics have the following functionality:

- Sequencing electronics for decoding the control signals to CCD drive signals
- CCD clock drivers and their overlap generation circuits
- Video amplifier with four selectable gains for CCD output signal processing
- CCD bias and supply voltage generation circuits
- CCD temperature control components

DEM operation is controlled by the Electronics Unit (ELU). The ELU sends the clock control sequence to DEM in real time, provides DEM supply voltages and receives the video signal from DEM. The Detector Module DEM, schematically illustrated in Figure 2.9, contains the circuits which are required to be in the proximity of the CCD. Cable length between ELU and CCD would have detrimental effects on the signals concerned if these circuits would be part of the ELU, and therefore these circuits are accommodated in the DEM.

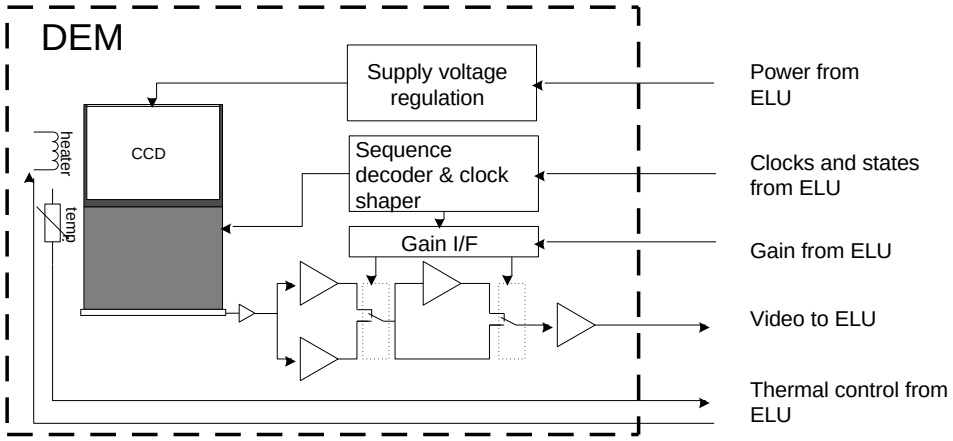

Figure 2.9 DEM electrical architecture *Courtesy of Fokker Space*

2.3. Electronic Unit

The main functions of the Electronics Unit (ELU) are to control the settings of the Optical Assembly, and to process the analogue video signal into digital video signals In order to synchronise these activities a discrete time period is used in the ELU, the so-called master clock period. The ELU receives its commands from the Interface Adapter Module, described in section 2.4. The digital output signal produced by the ELU is also send to the IAM.

2.3.1. Master Clock Period

The master clock signal is the heartbeat of OMI. It is used to synchronise all the activities of OMI in a discrete time period. This period is nominally set to two seconds, but it can be as long as six seconds. During one master clock period each CCD is read out multiple times (nominally five times). During each master clock period one digital video signal is send to the IAM.

2.3.2. Controlling the Optical Assembly

DEM Control

The DEMs are described in section 2.2.2. The two DEMs consist each of a CCD detector and electronics. The ELU controls the read-out sequence of the DEMs. This includes the read-out times of the CCDs, the gain settings of the DEMs, the binning factors, etc. The ELU also controls the temperature of the CCDs, by controlling the CCD heaters. The temperature is measured using a sensor in the CCDs. The ELU also provides the power for the DEMs.

Optical Bench Control

The optical bench, described in section 2.2.1, includes three mechanisms as well as a white light source and LEDs. The ELU controls the settings of the mechanisms, and switches the white light source (WLS) and LEDs on and off. Thus, the ELU supplies the power to the mechanisms and to the calibration lamps. By controlling the Optical Bench mechanisms and lamps, the ELU can switch between the nominal measurement and the various calibration measurements.

On the Optical Bench there are temperature sensors and two heater blocks. If the temperature of the Optical Bench drops below the desired minimum temperature, the ELU will switch the heaters on.

2.3.3. Video Signal Processing

From each of the two DEMs, the ELU receives an analogue video signal. This analogue signal is digitised using a 12-bit analogue-to-digital converter. During one master clock period, multiple digitised video frames are produced by the analogue-to-digital converter. All the video frames produced during one master clock period are co-added into one single frame. The process of co-adding reduces the amount of data send to the spacecraft, and at the same time the signal-to-noise is increased. Co-adding increases the size of the ground pixels in the flight direction.

2.4. Interface Adapter Module (IAM)

The Interface Adapter Module is the interface between the ELU, described in the previous section, and the Aura spacecraft. The purpose of the IAM is to make the OMI interface compliant to the interface of the spacecraft. The main functions of the IAM are:

- to process the commands it receives from the spacecraft and to send these to the ELU
- to format the telemetry it receives from the ELU and send it to the spacecraft
- to synchronise the clocks from the spacecraft and the ELU.

2.5. The performance of OMI

This section provides information on the expected performance of the OMI. Performance will be considered in terms of spectral calibration, radiometric calibration and signal-to-noise.

2.5.1. Radiometric Calibration

When studying the radiometric performance of the OMI, two products should be considered: the Level 1B *radiance* spectrum and the ratio of the Level 1B radiance and the Level 1B irradiance spectrum, here identified as the *reflectance* spectrum. As most algorithms that construct higher level products from the L1B data use the reflectance spectrum, radiometric calibration efforts are geared towards optimising this quantity.

The individual Level 1B radiance and irradiance products are calibrated using a number of measurements, including a NIST lamp and a stable white light source. The expected accuracy of the individual measurements is 3 to 4 percent depending on wavelength [*RD-2*]. The ratio of the two can be determined much more accurately, because the intrinsic uncertainty of the output of the NIST lamp is present in both measurements and will be cancelled. It is expected that the radiometric accuracy of the reflectance spectrum will be 1 percent [*RD-2*].

The radiometric calibration depends critically on the use of the diffusers, therefore their degradation will be monitored accurately.

2.5.2. Spectroscopic calibration

The assignment of a wavelength to a given CCD pixel, i.e. the wavelength calibration, is based on the accurate knowledge of the exact wavelength of a great number of Fraunhofer lines both in the radiance and in the irradiance spectrum. Details on this are given in section 3.3.2. For the performance of the wavelength calibration two terms should be considered: spectral stability and spectral knowledge. Due to thermal effects it is expected that the spectral calibration changes slightly along an orbit. This variability, the spectral stability, is expected to be on the order of $1/20^{th}$ of a pixel [*RD-2*]**.** The final result of the spectral calibration, i.e. the spectral knowledge, is obtained by using the Fraunhofer lines, and will be in the order of $1/100^{th}$ of a pixel [*RD-2*].

The spectral stability and the spectral knowledge will be different for the UV-1, UV-2 and VIS wavelength ranges. A performance issue related to the spectroscopic calibration is that

of the slit function determination. A special stimulus containing an Echelle spectrograph is used and the slit function will be sampled every 0.1 CCD pixel for a large number of locations on the CCD. Measuring the slit function can not be done routinely in-flight, so the assumption is that the slit function does not change over lifetime of OMI.

2.5.3. Signal-to-Noise

The ratio of the *useful signal* to the *noise signal* (i.e. the S/N ratio) of the Level 1B products is essential information for any algorithm that makes use of Level 1B data. Clearly the S/N ratio is a number that varies over time, e.g. due to instrumental effects, that depends on the viewing conditions and on the atmospheric conditions and furthermore is highly wavelength dependent. Moreover, the resulting S/N ratio will also depend on the number of binned rows. Therefore it is impossible to give a single number for the S/N. The values given for the S/N are the requirements as given in the Science Requirements Document [*RD-2*].

Table 2.3 The required S/N values, as taken from RD-2.

Wavelength range	**Critical trace gas**	**Required S/N (global mode)**	**Required S/N (spatial zoom-in mode)**
270 – 310 nm	O_3 profile	60 $(13 \times 48\ km^2)$	45 $(13 \times 24\ km^2)$
310 – 335 nm	O_3 column	265 $(13 \times 24\ km^2)$	190 $(13 \times 12\ km^2)$
335 – 365 nm	HCHO	1450 $(13 \times 24\ km^2)$	1050 $(13 \times 12\ km^2)$
365 – 420 nm	OClO	700 $(13 \times 24\ km^2)$	470 $(13 \times 12\ km^2)$
420 – 450 nm	NO_2	2600 $(13 \times 24\ km^2)$	1850 $(13 \times 12\ km^2)$
450 – 500 nm	$O_2 - O_2$	1400 $(13 \times 24\ km^2)$	1000 $(13 \times 12\ km^2)$

2.5.4. Other performance issues

Straylight

In UV/VIS satellite instruments straylight is a well-known problem, especially straylight from longer wavelengths that is detected at shorter wavelengths. As was pointed out, this was the major reason to divide the UV-channel into two separate channels, UV-1 and UV-2. Although this improves the situation considerably, straylight should still be corrected for. The straylight is expected to be smaller than 10 % before correction [*RD-2*]. After correction the straylight is expected to and to be reduced to 0.5 % at all wavelengths and swath angles [*RD-2*].

Spectral features

Since several retrieval methods which are developed for OMI will make use of specific (high frequency) spectral features in the reflectance spectrum, caused by high frequency variations in the absorption cross sections of the molecules, it is of paramount importance to prevent any spectrally dependent features caused by the instrument or its calibration. Spectral features resembling absorption features caused by the instrument and/or its calibration are expected to be less than 10^{-4} at all wavelengths and swath angles [*RD-2*].

Non-linearity

The read-out electronics – especially the CCD pre-amplifier- will cause some non-linearity in the conversion from the signal in [electrons] to [volts]. In particular in the UV channel this effect will be large, due to the fact that the intensity of the radiance varies by three

orders of magnitude over this channel. It is expected that after correction the non-linearity will be less than 0.2%, as defined in *RD-2*.

Geolocation

In the zoom-in mode OMI can measure pixel sizes of 13×12 km^2. This will enable OMI to monitor, a.o., tropospheric pollution on a regional scale and to look in between the clouds. The geolocation is expected to be known to $1/10^{th}$ of a ground pixel [*RD-2*]. Also a super zoom-in mode has been defined for geolocation calibration. In the super zoom-in mode the central 60 rows of the swath are read out unbinned. The total swath range covered in this mode is about 14 degrees, symmetric around the nadir-zero direction. These properties make the spatial super zoom-in mode well suited for geolocation validation.

2.6. Reference Documents (RD)

RD-1 Algorithm Theoretical Basis Document for Level 0 to 1B processing, *RP-OMIE-0000-FS-146*, issue 3, May 2001

RD-2 Science Requirements Document for OMI-EOS, *RS-OMIE-KNMI-001*, Version 2, December 2000. ISBN 90-369-2187-2, KNMI publication: 193

3. The Level 0 to Level 1B processor for OMI radiance, irradiance and calibration data

G.H.J. van den Oord[1], R.H.M. Voors[1], J. de Vries[2]
[1]Royal Netherlands Meteorological Institute (KNMI), De Bilt, The Netherlands
[2]Fokker Space, Leiden, The Netherlands

3.1. Introduction

In this chapter a description is given of the functionality of the Level 0 to 1B processor for OMI data. This processor is generally referred to as the OMI GDPS (Ground Data Processing Software). The input of the GDPS consists of Level 0 data as received from EDOS (EOS Data & Operations System). The output is Level 1B data that include geolocated and calibrated radiances, calibrated irradiances, and calibration measurement results. Radiance and irradiance products are used in the Level 1B to 2 processing, the calibration data are used for deriving correction parameters used in the 0 to 1B processor and for monitoring the instrument's performance (see Chapter 4).

The OMI GDPS is developed by an industrial contractor (Fokker Space) under contract by the Netherlands Agency for Aerospace Programmes (NIVR). Fokker Space is also the prime contractor responsible for the OMI hardware and instrument calibration. In order to achieve a sound development process of the processor the *ESA S/W Engineering Standard for Small Software Projects* [RD-1] was applied. The development process is described in the *Software Management Plan* (SMP) [RD-2]. The user requirements applicable to the processor are described in the *User Requirements Document* (URD) [RD-3]. The algorithm steps are described in the *Algorithm Theoretical Basis Document* (ATBD) [RD-4]. The software requirements and the architectural design are described in the *Software Specification Document* (SSD) [RD-5]. The *Detailed Processing Model and Parameter Data List* (DPM/PDL) [RD-6] describes the algorithms as implemented in the processor while the *Input/Output Data Specification* (IODS) [RD-7] describes the input to the processor and its output, the Level 1b data products. Finally the GDPS *Verification and Validation Plan* (SVVP) [RD-8] describes the tests to be performed during development on unit and system level, the integration tests and the acceptance tests.

Under the contract a Prototype Version, an Engineering Version and a Launch Version are developed. Only the Launch Version is a contractual deliverable. The development process is structured by various milestones in the form of reviews: the User Requirements Review (9 July 1999), the Software Requirements / Architectural Design Review (6-7 April 2000), the Detailed Design Review (31 May & 1 June 2001) and the Software Transfer Review (2002). Between reviews the documentation is frozen but in preparation for a review basically all documents are updated. This reflects the evolutionary approach of the development process.

Because details about the GDPS are extensively described in the reference documents mentioned above [RD-2 – RD-8], we present in the present document only a high level description of the 0 to 1B processing algorithm, thereby making a trade-off between the level of detail and the accessibility of the information provided. Details can be found in the ATBD [RD-4]. In this chapter a description of the GDPS at the time of writing is given. Various steps in the processor may be modified at a later stage, if required by the actual performance of the OMI Flight Model as determined during performance verification and calibration.

3.2. The forward model

In this section a forward model for the signal flow through the instrument is presented. This forward model serves as a guide for the inverse model discussed later.

OMI can be considered as a system with four components:

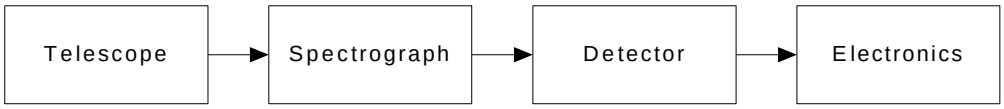

Figure 3.1 Schematic representation of the OMI system

In the following a systematic description is given of all four elements, in terms of the signal flow through each element.

3.2.1. Telescope

There are three different ways in which light can pass through the OMI telescope:

1. light can enter the telescope through the nadir port, through aperture 001, is then reflected off the primary mirror (103), goes through the scrambler (005) and is then focused by the secondary mirror (007) on the spectrograph slit (008).
2. light can enter via the sun port, passes through the mesh, then falls on one of the three reflection diffusers, is reflected off the folding mirror C03 towards the scrambler, from where it follows the same path as light that enters through the nadir port.
3. light from the on-board White Light Source is reflected off mirror C10, transmitted through the transmission diffuser C05 and after reflection off the folding mirror C03 follows the same path as that of a solar light beam.

These three different light paths result in three different descriptions of the signal that is incident on the spectrograph slit:

Radiance measurement:

$$S_{slit}(l,a,t) = S_{earth-radiance}(l,a,P,t)R_{tel\_earth}(l,a) \qquad [photons/s.rad.nm] \qquad [3\text{-}1]$$

Irradiance measurement:

$$S_{slit}(l,a) = S_{solar-irradiance}(l) \times BRDF \times R_{tel\_sun}(l,a) \qquad [photons/s.rad.nm] \qquad [3\text{-}2]$$

WLS measurement:

$$S_{slit}(l,a) = S_{wls}(l,a)R_{tel\_WLS}(l,a) \qquad [photons/s.rad.nm] \qquad [3\text{-}3]$$

Here l is the wavelength, a the swath angle, P the polarisation state of the incident light, t is time, and *BRDF* is the Bidirectional Reflection Distribution function of the internal diffuser. The different R's indicate the specific throughputs of the different optical paths. A key design element in OMI is the choice to have the primary mirror made of the same material as the folding mirror so that R_{tel_earth} is equal to R_{tel_sun}. The throughput functions are independent of polarisation state of the incident light because of the polarisation scrambler, and a design property of the first scrambler surface that serves to compensate for polarisation effects induced by the primary mirror.

For radiance observations, the nadir direction is imaged at the centre of the spectrograph slit and the extreme swath angles at the edges of the slit. For irradiance observations, the slit receives light from different parts of the diffuser, as a function of position along the slit. The illumination across the slit is always homogeneous, by design.

3.2.2. Spectrograph

The spectrograph projects an image of the slit on the detector while dispersing the signal in the spectral direction. This can be described by a multiplication with the throughtput-function of the specific channel optics ($R_{channel\_optics}$ for UV-1, UV-2 and VIS)) and a convolution with the slit function (r_{chan})*:*

$$S_{useful}(l,a,t) = \int S_{slit}(l',a,t) R_{channel\_optics}(l') r_{chan}(l-l',a)\,dl' \quad [photons/s.rad.nm] \quad [3\text{-}4]$$

Note that each (sub-)channel has its proper slitfunction as is reflected in the different spectral resolutions. The slit function also varies slightly as a function of swath angle a .

Unwanted internal reflections (e.g., off the grating) will cause out-of-band (spectral) and/or out-of-field (spatial) straylight. The amount of straylight scales with the amount of useful light, often in a very complex way. Symbolically we can write:

$$S_{total} = S_{useful} + S_{straylight}(S_{useful}) \qquad [3\text{-}5]$$

3.2.3. Detector

Charge generation

The number of photons per second incident on a given CCD pixel (i,j) can be written as a convolution of the signal, expressed in wavelength and viewing angle co-ordinates, with the pixel response function (PRF):

$$S_{total}(i,j,t) = \iint S_{total}(l',a',t) \cdot PRF_i(l'-l) \cdot PRF_j(a'-a) \cdot dl' \cdot da' \quad [photons/s] \quad [3\text{-}6]$$

As a result the signal is expressed in CCD co-ordinates rather than in wavelength and viewing angle co-ordinates. The PRF of a pixel gives the response of that pixel as a function of position relative to the center of the pixel. The typical Full Widths at Half Maximum of a PRF in the two relevant CCD directions determine the spectral and spatial sampling distances of a pixel.

The photons incident on a CCD pixel create free electrons at a rate proportional to the quantum efficiency. For an exposure time Δt the number of electrons equals:

$$S_{electrons}(i,j) = S_{photons}(i,j,t) \cdot \overline{QE}(l) \cdot PRNU(i,j,l)\Delta t \quad [electrons] \qquad [3\text{-}7]$$

In this expression the quantum efficiency (QE) is described as an average quantum efficiency, at a specific wavelength, times a pixel-specific Pixel Response Non-Uniformity (PRNU). The PRNU is a dimensionless number of the order of unity that expresses the difference in quantum efficiency of a given CCD pixel, relative to the average quantum efficiency at the typical wavelength of a column of CCD pixels.

A second source of charge generation in a pixel is dark current. The amount of dark current is a simple function of temperature and doubles, roughly, every five degrees Kelvin. The standard deviation of the dark current distribution on a CCD is the so-called Dark Signal Non-

Uniformity (DSNU). For the OMI CCDs there is only a very slight difference between the dark current distributions in the image area and in the (masked) storage area.

Charge transfer

The OMI CCDs are frame-transfer CCDs and a discussion of the transfer of charges is facilitated by using the picture of potential wells travelling over a fixed grid of CCD pixels. In each pixel, in which a well resides for some time, the amount of electrons contained in a well changes due to illumination by photons and/or dark current. The transfer of a well over the CCD occurs in six steps:

1. rapid transfer of the well from the top of the CCD to the pixel location in the image area where the exposure takes place.
2. exposure to 'useful' signal (actual measurement of duration Δt).
3. rapid transfer from image region to corresponding location in storage region.
4. (slow) vertical transfer through storage region, towards the read-out register.
5. transfer of the well into read-out register. Multiple wells, that is, multiple CCD rows, are added in the read-out register (binning).
6. horizontal transfer through the read-out register towards the output capacitance at which the charge content of a well is measured in terms of a voltage over the capacitance.

During each of these steps the dark current contribution in a well increases proportional to the time the well spends in a specific pixel and the (typical) dark current of that pixel.

During steps 1 and 3 the well moves rapidly over the image area of the CCD. Because this area is illuminated during these transfers, unwanted charge is added to the well. This unwanted charge is called the smear signal. For a constant illumination it corresponds to the integrated signal along a CCD column times the ratio of the frame transfer time over the exposure time. Furthermore, the image areas of the OMI CCDs have a few masked rows at the top of the CCDs and near the image area. The wells that have their useful exposure (step 2) in these masked pixels contain in the end only information about the smear signal (next to dark current signal). This information can also be used for correction of the smear effect.

When a well moves to the next pixel a tiny fraction of the charge in the well is left behind. At the same time the well picks up some charges left behind by the preceding well. This effect is related to the charge transfer efficiency (CTE) of the CCD pixels. For the OMI CCDs less than 1% (on average about 0.5-0.7%) of charge injected at the top of a CCD does not arrive at the output capacitance. For charges injected in the lower part of the image area the amount of charge left behind is even less. Because the charge in a well changes continuously, because of illumination and/or dark current, modelling of CTE effects involves considerable bookkeeping. Both numerical and analytical models have been developed in the OMI project that describe CTE effects on the useful signal, on the smear signal and on the dark current. A CCD image can be modelled in terms of CTE-matrices acting on the photon and dark current generated signal.

In summary, the signal flow on a CCD depends on the dark current build-up, the useful signal incident on the CCD, the smear signal and the charge transfer effects. Both analytical models and computer simulations have been developed to model these effects.

3.2.4. Read-out electronics

When the signal reaches the read-out electronics, the accumulated charge is converted to an analogue voltage at the capacitance of the CCD. The CCD pre-amplifier causes a small non-linearity in this process. The signal is further amplified by the DEM-amplifier that sets the gain, and the Correlated Double Sampler (CDS):

$$S_{Volts}(i,j) = S_{electrons}(i,j) \cdot f_{CCD} \cdot L(S(i,j)) \cdot f_{DEM}(i,j) \cdot f_{CDS} \qquad [Volt] \qquad [3\text{-}8]$$

Here f_{CCD} is the charge-to-voltage conversion factor, the function $L(S(i,j))$ describes the non-linearity, f_{DEM} describes the gain factor and f_{CDS} is the CDS gain.

The signal is then converted from an analogue video signal to a digital signal as follows. The CDS samples both the (useful) video signal and a reference level and subtracts these samples to minimise read-out noise. To the resulting signal a small, gain-dependent, offset voltage O_{CDS} is applied to ensure a positive signal:

$$S_{Volts}(i,j) = S_{Volts}(i,j) + O_{CDS} \qquad [Volt] \qquad [3\text{-}9]$$

The resulting voltage is then fed into the 12-bit Analogue-Digital Converter that converts the analogue signal from [Volts] to digital counts[ADC counts]:

$$S_{ADC}(i,j) = S_{Volts}(i,j) \cdot f_{ADC} \qquad [ADC\ counts] \qquad [3\text{-}10]$$

A number of individual CCD read-outs (images) will normally be co-added in the 16-bit co-addition register.

$$S_{co-added}(i,j) = \sum_{n\_coadditions} S_{ADC}(i,j) \qquad [Counts] \qquad [3\text{-}11]$$

The co-added signal is the output of the read-out electronics. This signal is, after some data formatting by the ELU, sent to the IAM.

3.3. The inversion of the forward model

3.3.1. Correction steps for calibrated radiances and irradiances

In this section, a summary of the correction algorithms present in the GDPS is given, as well as the order in which they are executed.

The inversion of the forward model in the GDPS involves twelve *correction algorithms* for radiances and one additional for irradiances. All correction algorithms use correction parameters stored in the so-called Operational Parameters File (OPF). The straylight and smear correction algorithms also use the actual signal on the CCD. The parameters stored in the OPF result from the on-ground and in-flight calibration activities as described in Chapter 4. The choice to use correction parameters from an OPF in stead of the actual measurement is driven by the fact that the parameters in the OPF are derived from numerous (calibration) measurements and, therefore, have a better precision than correction parameters based on a single measurement. However, the processor also contains a number of *flagging algorithms* that set flags in the data product when a measured parameter deviates too much from its OPF value. Next to the correction algorithms and the flagging algorithms the GDPS also contains *calculation algorithms* that are used to evaluate OPF parameters for each measurement. Such an evaluation consists of applying, e.g., wavelength, binning factor or temperature corrections to an OPF parameter. Calculation algorithms in general evaluate OPF parameters for use in correction and flagging algorithms.

The correction steps involved are listed below. Step 13 only applies to irradiances. For the trivial and straightforward correction steps a short description is provided.

1. Co-addition division: division by number of co-added images (Eq. 3-11).
2. ADC conversion: division by the ADC conversion factor (Eq. 3-10).
3. Offset correction: subtraction of the gain-dependent offset voltage (Eq. 3-9)
4. Electronic conversion: division by appropriate electronic gain ratio to convert signal to reference gain factor unity (Eq. 3-8). A non-linearity correction is applied based on the evaluation of a fourth order polynomial. Note that $f_{CCD}\, f_{DEM}\, f_{CDS}$ is only used as a combination because each of the factors can only be evaluated individually on unit level.
5. Binning factor division: division by the binning factor used in the read-out register.
6. Dark correction: subtraction of a dark current image obtained with identical CCD clocking settings as the measurement to which it is applied. This insures that the dark current build-up and the charge transfer effects are properly corrected for. A calculation algorithm evaluates the OPF dark current image for the CCD temperature at the time of measurement. Note that the temperature dependence of the dark current is accurately known.
7. Charge transfer efficiency correction: first all CCD rows, each stored as a vector, are multiplied by the inverse CTE response matrix for horizontal charge transfer in the read-out register. Then all CCD columns, each again stored as a vector, are multiplied by the inverse CTE response matrix for vertical charge transfer. In case of binning, the response matrix for that pixel, in a collection of binned pixels, that is closest to the readout register is used.
8. Exposure smear correction: subtraction of smear contribution. In the OPF the users can set a parameter to pre-select the correction algorithm that will be applied. One algorithm subtracts the integrated signal along a CCD column multiplied by the ratio of the frame transfer time (4.32 ms) and the exposure time (nominally 0.4 s). This algorithm is exact in case of constant illumination (in time). The second algorithm is based on a linear interpolation over the CCD (in the swath direction) between the smear signal in the masked upper and lower dark rows. This algorithm corrects to some extend for time variations in the scene. Because the smear contribution is very small it is expected that the second method has a reduced accuracy and that the first method will be used.
9. PRNU correction: divides the CCD image by a PRNU map (Eq. 3-7). In this way the pixel-to-pixel variations in quantum efficiency at a specific wavelength are accounted for. Note that the average quantum efficiency is implicitly contained in the radiance sensitivity correction (step 12). For binned images the average PRNU values of the binned pixels are used in the algorithm. This corresponds to the approximation that each of the binned pixels has received an equal number of photons.
10. Exposure time division: division by the exposure time used (Eq. 3-7).
11. Straylight correction: see discussion below (Eq. 3-5).
12. Radiance Sensitivity correction: multiplication with the radiance sensitivity function (Eqs. 3-1, 3-4, 3-6 and 3-7). The radiance sensitivity function as obtained from the on-ground calibration is stored in the OPF as function of swath angle and wavelength. It is assumed that the swath angle dependence will not change in-flight. However, the

wavelength calibration of a pixel will show small variations due to temperature variations of the Optical Bench along the orbit. Therefore the radiance sensitivity function is interpolated to the wavelength grid of the actual measurement. Currently this is a simple linear interpolation but other schemes (e.g., cubic spline) are under investigation.

13. OMI BRDF conversion: division by BRDF (Eq. 3-2, applies only to irradiance measurements). The BRDF is stored in the OPF as a function of solar azimuth angle, solar elevation angle and wavelength. The same wavelength interpolation as discussed in step 12 is applied.

The straylight correction algorithm (step 11) for OMI is currently not determined. Results from the OMI Development Model (DM) indicate that only very weak features related to spatial straylight are present. Most of the straylight observed is spectral in nature with about 20% in the UV-1 and less than 1 % in UV-2 (the OMI DM does not have a VIS channel). Because the OMI PFM will have a straylight suppression coating on the secondary telescope mirror the performance in the UV-1 is expected to improve further. The currently foreseen straylight algorithm is derived as follows. The straylight signal on the CCD can be described as

$$S_{stray}(l,a) = \int_{swath} \int I_{useful}(l',a') r(l,l';a,a') dl' da' \qquad [3\text{-}12]$$

with $I_{useful}(l,a)$ the incoming signal as function of wavelength and swath angle and $r(l,l';a,a')$ the straylight response function. In discrete form this can be written as:

$$S_{stray,i,j} = \sum_k \sum_l I_{l,k} r_{i,l;j,k} \Delta l_l \Delta a_k \qquad [3\text{-}13]$$

When spatial straylight is not important (which is not known in detail yet) all functions become independent of the swath angle, so $S_{stray,i} = \sum_l I_l r_{i,l} \Delta l_l$. The components of $r_{i,l,j,k}$ (the so-called straylight factors) will be determined during the calibration of OMI. The total signal on the CCD is a combination of useful signal and straylight. Combining the formal expressions for these signal permits to derive a straylight correction in the form of a multiplication of a straylight correction matrix times the observed signal stored in a vector

$$S_{measured,i} = S_{useful} + S_{stray} = I_i R_i + \sum_l I_l r_{i,l} \Delta l_l \qquad [3\text{-}14]$$

with R_i the radiance sensitivity function (as used in correction step 12 above).

3.3.2. Spectral calibration

The procedure for spectral calibration is based on the fact that the spectral calibration of OMI will change only slightly as a function of the temperature of the Optical Bench (OPB). Furthermore, OMI will provide a very stable thermal environment with a high repeatability of the OPB temperature along the orbit. Therefore it has been decided to parameterise the wavelength calibration as a function of OPB temperature.

The OPF contains wavelength polynomial coefficients for all image rows (including for various binning factors) for a given reference temperature of the OPB. The OPF also contains polynomial coefficients to evaluate the wavelength polynomial coefficients at different OPB temperatures. The temperature of the OPB at the time of a measurement, as measured by

thermistors, is used to calculate corrected wavelength polynomial coefficients for each image row, that is, for each (ir)radiance spectrum. These corrected wavelength polynomial coefficients are provided in the Level 1B radiance and irradiance products. The reason for providing wavelength polynomial coefficients in the Level 1B data products, in stead of providing actual wavelengths, is that it considerably reduces the size of a data product.

The above mentioned steps imply that, in operational sense, the GDPS simply takes wavelength polynomial coefficients from the OPF, evaluates these for the OPB temperature at the time of measurement, and outputs the result in the Level 1b (ir)radiance product.

However, for each measured (ir)radiance spectrum the GDPS also performs a wavelength calibration. The result of this calibration, in terms of wavelength polynomial coefficients, is stored, together with the OPB temperature, in the Level 1B Calibration product. This product is used in off-line analyses to derive and monitor the wavelength and OPB-temperature polynomial coefficients contained in the OPF. The rationale for this approach is that the spectral calibration, resulting from many spectral fits, is anticipated to be more accurate than the spectral calibration obtained from an individual measurement.

The spectral calibration that is performed on each spectrum is based on a fit of the Fraunhofer structures in optimised spectral windows in the UV-1, UV-2 and VIS channel. Typically 6 to 21 windows are used in a channel. The central wavelengths of these windows are determined by the fits. Then a polynomial fit is performed over each (sub-)channel and the resulting polynomial coefficients are written to the Level 1B Calibration product (evaluation of a polynomial gives wavelength as function of CCD pixel column number).

Each (non-linear) fit is based on minimising, in chi-square sense, the differences between a high-resolution solar spectrum, convoluted with the OMI slit function and therefore at OMI resolution, and the measured spectrum in a window. For radiance measurements it is possible to include an ozone cross-section and a Ring contribution in the fit (both at OMI resolution).

Of paramount importance for the above outlined approach is that during the on-ground calibration period the slit function of OMI will be measured on pixel level. The combination of an accurately known slit function, together with a high-resolution solar spectrum, provides the required spectral knowledge. Simulations indicate that the requirements for spectral calibration can be met for typical signal-to-noise factors. The results of thermal cycling of the OMI PFM will be used to validate the approach for spectral calibration.

3.3.3. Geolocation calibration

Based on the elevation and azimuth angles for each pixel line-of-sight, the time of measurement and the spacecraft ephemeris the SDP toolkit [RD-9] is used to determine the geolocation of the centre of each groundpixel. In the flight direction the time stamp at the middle of all co-added exposures is used. In the swath direction an interpolation of the lines-of-sight of binned pixels is used. Note that the (binned) pixels lines-of-sight are given with respect to the spacecraft alignment cube. The spacecraft attitude data serves as an external input to geolocation calculation.

In addition to geolocation the Level 1b radiance product will also contain other relevant information such as solar zenith angles, terrain height and sun glint possibility flagging.

3.4. Summary

In Figures 3.2 to 3.4 we show the data processing flow for radiance and irradiance measurements as discussed in the previous section (these figures are based on diagrams provided by Fokker Space). Figure 3.2 shows the part of the processing that is equal for both Sun and Earth measurements. The other two figures show the remainder of the processing flow for Sun

and Earth measurements separately. The steps that are taken in the conversion of raw measurement data to Level 1B data, are shown in the left column. That column contains the previously discussed *correction algorithms*. The columns to the right contain the *calculation* and *flagging algorithms*. Similar diagrams exist for WLS, LED and Dark measurements, but since these measurements are performed for calibration purposes, these diagrams are not discussed here.

More details about the corrections applied can be found in RD-4, including an error budget.

3.5. Reference Documents

RD-1. ESA S/W Engineering Standard for Small Software Projects, *ESA PSS-05-01, issue 2*, February 1991
RD-2. Software Management Plan (SMP) for the OMI Level 0 to 1B Data Processor, *PL-OMIE-7000-FS-187*, issue 2, March 2000
RD-3. User Requirements Document (URD) for the OMI Level 0 to 1B Data Processor, *RP-OMIE-7000-FS-186*, issue 3, May 2001
RD-4. Algorithm Theoretical Basis Document for Level 0 to 1B processing, *RP-OMIE-0000-FS-146*, issue 3, May 2001
RD-5. Software Specification Document (SSD) for the OMI Level 0 to 1B Processor, *SD-OMIE-7200-FS-250*, issue 2, May 2001.
RD-6. GDPS Detailed Processing Model and Parameter Data List (DPM/PDL), *SD-OMIE-7100-FS-251*, issue 2, May 2001
RD-7. Input/Output Data Specification (IODS), *SD-OMIE-7200-FS-275*, issue 2, May 2001
RD-8. GDPS Verification and Validation Plan (SVVP), *PL-OMIE-7000-FS-304*, issue 2, May 2001
RD-9. NASA, SDP toolkit, version 5.2.7, NASA: http//:edhs1.gsfc.nasa.gov

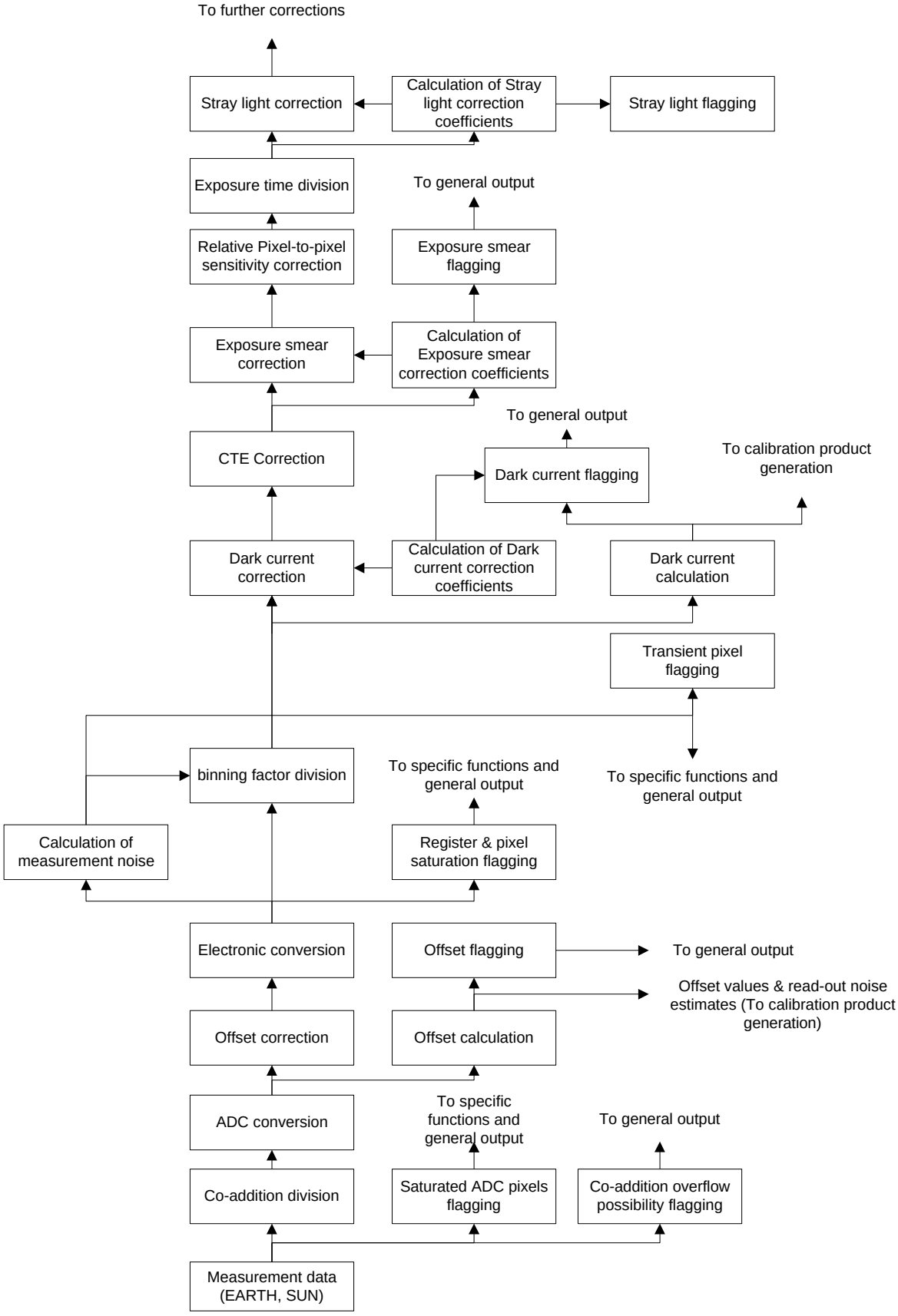

Figure 3.2: Generic science data processing flow for both Sun and Earth measurements.

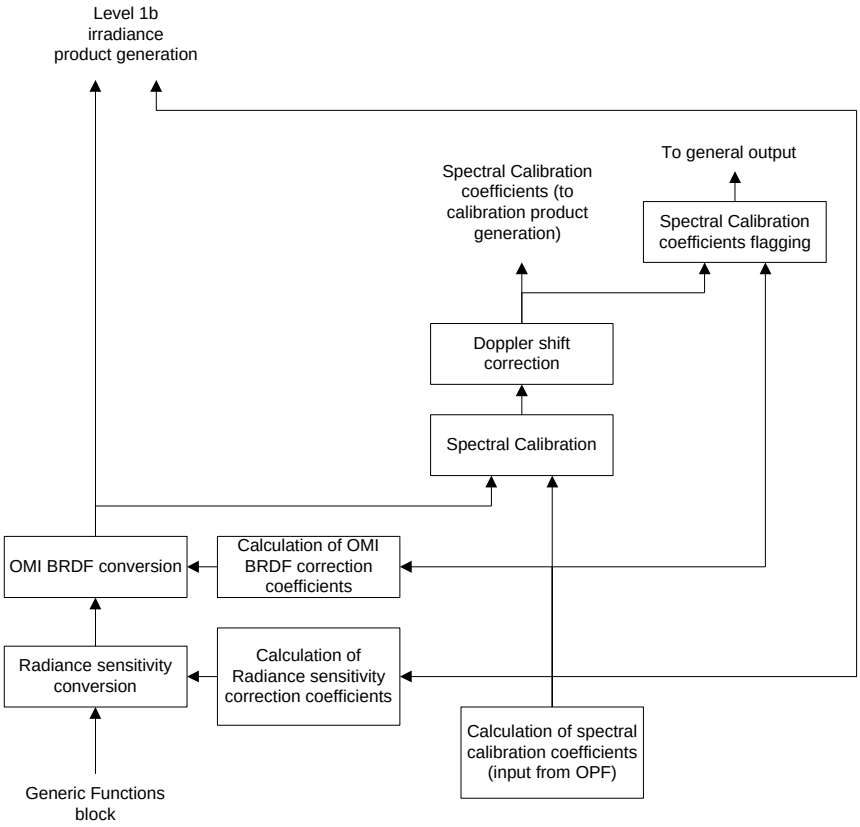

Figure 3.3: Science data processing flow for Sun measurements

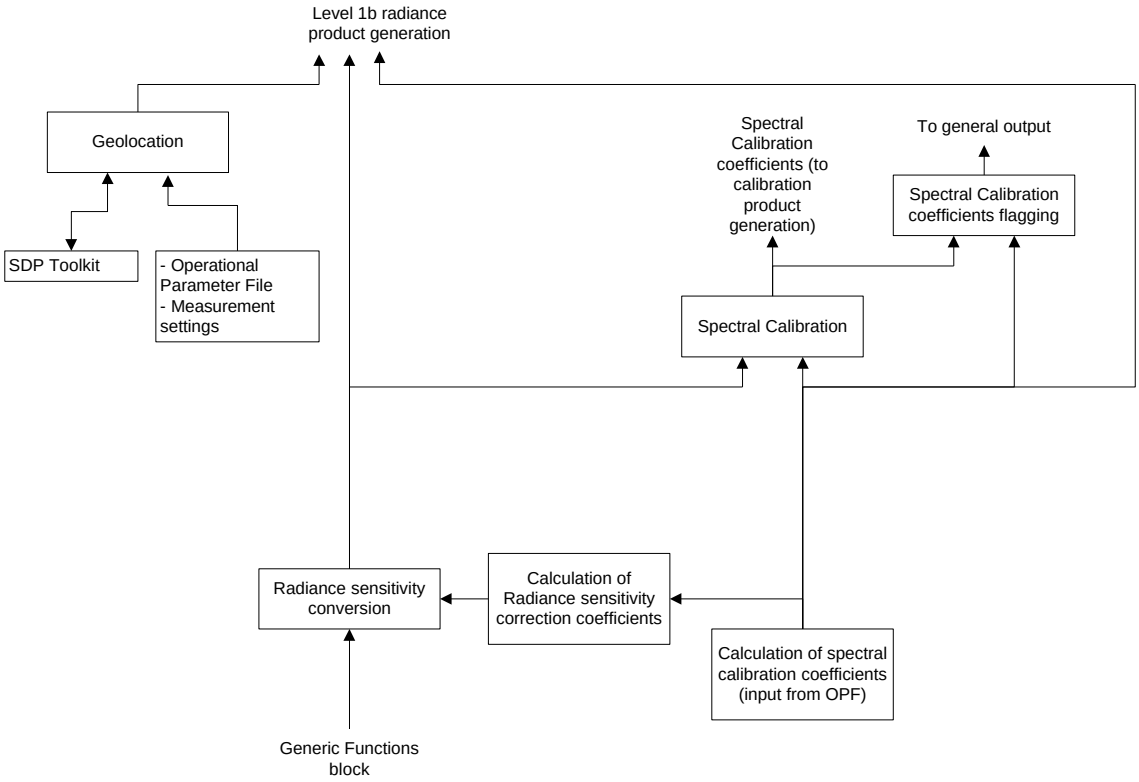

Figure 3.4: Science data processing flow for Earth measurement

4. OMI Calibration and Characterisation

R.H.M. Voors[1], M.R. Dobber[1] en R.J. Dirksen[1]
[1]Royal Netherlands Meteorological Institute (KNMI), De Bilt, The Netherlands

4.1. Introduction

In this section an overview is given of the calibration and characterisation efforts that are planned for the OMI. The core result of these efforts will be the Operational Parameters File (OPF). This file is contains the information needed to run the Level 0 to 1B processor. This chapter provides information on how the parameter values that end up in the OPF are obtained. The information given in this chapter is an extract from more extensive documents in which the calibration and characterisation procedures of the OMI are described. The most important of these are: the *Calibration Plan* [RD 1] and the *ATBD for Level 0 to 1B processing* [RD 2].

In terms of operations, the necessary parameter values will be provided by the calibration scientist and will be put into the OPF after an OSAB decision. The calibration scientist will extract information from both on-ground and in-flight measurements. These measurements will be stored in separate databases. The connections of the OPF to other relevant products and processors are shown in Figure 4.1.

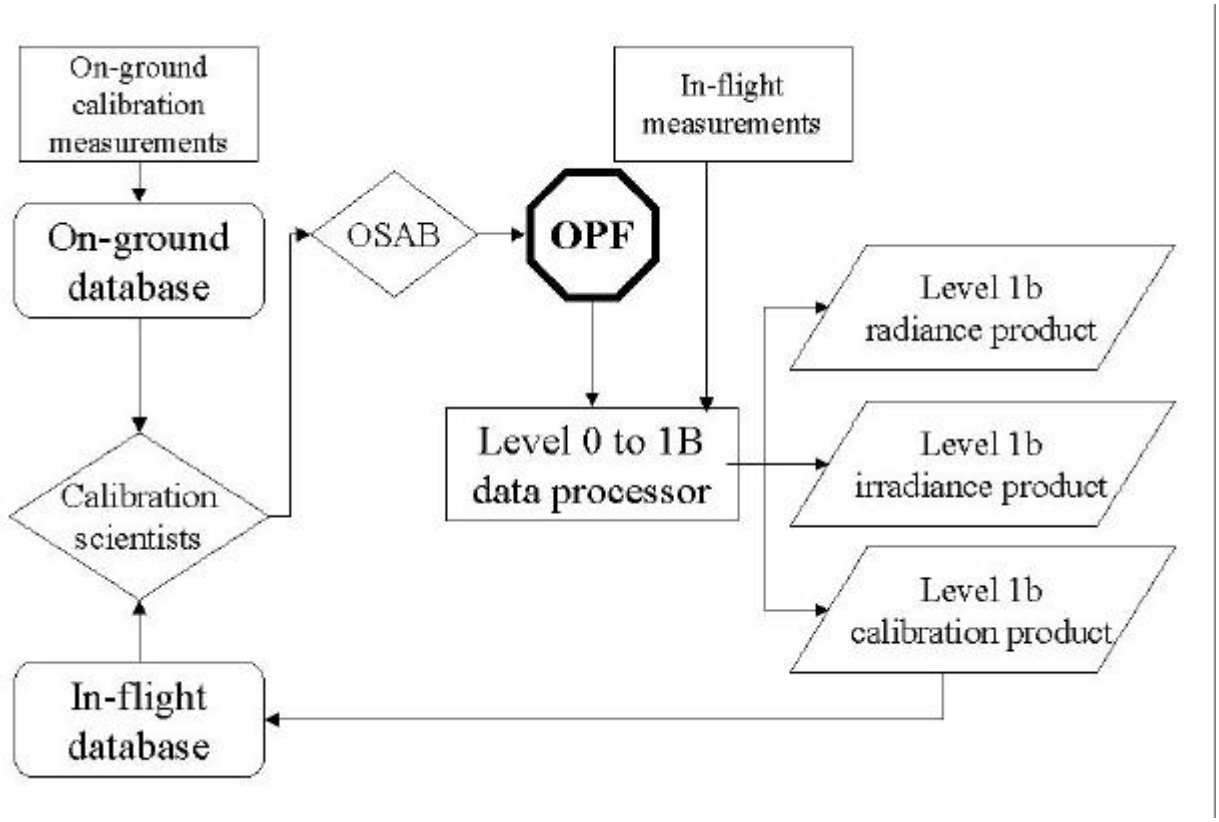

Figure 4.1 The relation of the Operational Parameters File to the relevant products and processors.

In principle the calibration of OMI is very simple: for each CCD pixel it should be determined to which wavelength it corresponds (wavelength calibration) and to which location on the ground (geo-location). The final step is the radiometric calibration of the digitally read out counts.

Wavelength calibration

This is the assignment of a vacuum wavelength to a given CCD pixel. The initial calibration is done by using a spectral line source. More accurate wavelength calibration is done in-flight using Fraunhofer lines in both Sun and Earth spectra (see Section 3.3.2).

Geo-location

This is the assignment of the geo-physical co-ordinates to CCD pixels. The viewing direction for every detector pixel (pixel line of sight, PLOS) and the pixel field of view (PFOV) function can be determined using the star simulator stimulus (see section 4.3.3) over the total field of view (TFOV). The edges and sharpness of the TFOV through the nadir port can be determined via rotation of the instrument, mounted on a turn-tilt table, over a range covering -60° to +60°. To determine the PFOV this scanning will be done in 1° steps over the complete range. An estimate of the PFOV function can be made with smaller scanning steps, typically 0.1°. This will be done for about 10 regions on the CCD. The FOV of about 0.8° in the flight direction will be measured by scanning perpendicular to the nadir direction. By tilting the turn-tilt table, a scan over 1.2 ° will be made, at a nominal range from position -0.6° to +0.6° with 0.1° steps. Pointing parameter values of the spacecraft are provided by NASA.

Radiometric calibration

This is the conversion from digitally read-out counts to physical units, i.e. photons/s.sr.cm^2.nm for earth radiance measurements and photons/s.cm^2.nm for sun irradiance measurements. This involves the determination of two main functions: the radiance sensitivity function (conversion from digital numbers to photons/cm^2.sr.cm) and the bi-directional reflection distribution function (BRDF) (expressed in 1/sr) of the OMI instrument. There are 3 instrument BRDF functions, one for every on-board reflectance diffuser. Each of these 3 instrument BRDF functions is mainly determined by the component level BRDF of the corresponding on-board diffuser. Both the radiance sensitivity function and the BRDF are determined by using a very stable white light source that simulates the in-flight illumination environment. For the radiance sensitivity function calibrated external diffusers are employed in addition.

An absolutely calibrated NIST lamp is used for absolute radiometric calibration (in conjunction with calibrated external diffusers for absolute radiance calibration). In addition, the following detector properties have to be determined and corrected for, in the radiometric calibration: co-addition, ADC, offset, electronic conversion, binning factors, CTE, dark current, exposure smear, pixel-response non-uniformity (PRNU) correction, exposure time and stray light (see Section 3.3).

4.2. The contents of the Operational Parameter File

In the previous chapter the subsequent steps are described that are taken to go from a raw level 0 file to a fully calibrated and geo-located level 1B file. For all these individual steps parameter values are needed that are provided by the OPF.

Table 4.1lists the most important of these parameters and indicates from which measurement their values are derived. It is not the intention to provide a complete list. In the next section these measurements are described in more detail.

Table 4.1: List of the most important parameters in the OPF that are the result of on-ground or in-flight calibration measurements.

OPF parameter	How obtained	When obtained (1)
ADC conversion factor	VTT/Finavitec	P
Offset	zero-second Dark, read-out register	P + I
Electronic conversion factor (incl. non-linearity)	VTT/Finavitec + LSS	P + I
CTE	Dark + WLS	P + I
Dark current	dedicated Dark measurements	P + I
PRNU	WLS	P + I
Exposure time	VTT/Finavitec	P
Stray light	Stray light experiments	P + I
Radiance sensitivity	NIST FEL	P
BRDF	WLS-A, sun	P + I
Wavelength calibration polynomial	Spectral Line Source, Sun, Earth	P + I
Slit function	Slit function measurement stimulus	P
Geo-location parameters	Star simulator stimulus	P + I

Note: (1) P: pre-flight, I: in-flight

4.3. Description of the On-ground measurements

For the on-ground calibration, a number of purpose-built stimuli are available for the calibration and characterisation of the instrument. Below, a description of each stimulus is given and it is also indicated for which calibration measurement it is used. Most stimuli can also be used to measure spatial (out-of-field) straylight. A summary is given Table 4.2.

4.3.1. White Light Stimulus (WLS-A)

This light source gives an unpolarised collimated (0.5°) temporally stable white light (Xe) beam. In its standard configuration it is a sun simulator that can be used for sun irradiance measurements, both under ambient and vacuum conditions. Using a calibrated reflection diffuser, this stimulus will also be used to perform radiance calibration measurements. The ratio of these two provides the BRDF of the OMI.

4.3.2. Linearity and stray light stimulus (LSS)

This stimulus emits unpolarised white light and gives a complete FOV illumination. Light will enter the instrument through the calibration port (at the location of mirror C09, see Figure 2.4) and will illuminate the transmission diffuser C05. When used with a set of cut-off filters, it is used for determining the characteristics of spectral (out-of-band) stray light. When used with a set of neutral density (ND) filters it is also used for non-linearity characterisation.

4.3.3. Star simulator stimulus

This stimulus consists of a white light source, which is highly collimated to a 2 arcmin ($1/7^{th}$ of a pixel) beam. Its main purpose is to measure the total and pixel FOV and LOS performance (geo-location). It is also used to determine spatial polarisation effects: a narrow beam of light that passes through the diffuser will be imaged on the spectrograph slit as 4 narrow spots, with two perpendicular polarisation directions (this spatial effect is caused by the scrambler and is called the “wybertje” or “diamond” effect). The spatial separation of these

beams is very small (~1/3rd of a pixel in swath direction) and is not expected to have a significant effect on the quality of the measurements.

Table 4.2: Summary of the available stimuli, used for the on-ground calibration of OMI. Listed are the most important quantities that will be determined using these stimuli.

Stimulus	Quantity
White Light stimulus A	▪ BRDF radiance/5° ▪ BRDF irradiance/0.5° ▪ Out of field stray light
Linearity and stray light stimulus	▪ Linearity checks over ~4 decades ▪ Out of band stray light per filter ▪ Out of band stray light <1000nm ▪ CCD memory/saturation effects
Star stimulus	▪ Total FOV, spatial, range ±65° ▪ FOV flight direction, range ±1° ▪ Instrument LOS ▪ Pixel FOV ▪ Pixel LOS, relative, from PFOV ▪ Out-of-field stray light on pixel and total FOV scale ▪ Spatial polarisation effects
Spectral Line Source stimulus	▪ Wavelength range per channel ▪ Spectral sampling
Slit function measuring stimulus	▪ Slit function, resolution 0.03-0.05 nm (0.1 pixel)
Polarisation Stimulus	▪ Scrambler performance
NIST FEL lamp	▪ Absolute radiance/5°, range ±65° ▪ Absolute irradiance/2°, range ±12°

4.3.4. Spectral line source stimulus

This stimulus contains a Pt-Cr-Ne hollow cathode lamp. The beam illuminates the transmission diffuser C05 through the OMI calibration port. It will be used to obtain the initial wavelength calibration.

4.3.5. Slit function measurement stimulus

This stimulus consists of a white light source that illuminates an echelle spectrograph, which in turn will output 10 beams with a different central wavelength (corresponding to 10 high orders of the echelle grating) with a very narrow wavelength bandwidth (0.03 to 0.05 nm, approximately 1/10th of a pixel). The central wavelength of these beams will be shifted by small amounts (~0.03 nm) to illuminate different sections of an individual CCD pixel. Light from this stimulus will enter through the calibration port, which ensures that the entire swath will be illuminated at once. This stimulus will be used to measure the (spectral) slit function of the OMI very accurately.

4.3.6. Polarisation stimulus

This stimulus consists of a collimated (3 degrees) white light source, which is polarised using a rotatable Brewster angle reflection polariser. It will be used to measure the performance of the polarisation scrambler.

4.3.7. NIST FEL lamp

This stimulus consist of a 1000 Watts NIST calibrated FEL tungsten-halogen lamp. It will be used for the absolute radiance and irradiance calibration. Together with WLS-A they comprise the main sources in the radiometric calibration procedure.

4.3.8. Dark measurements

The dark signal will be studied for different exposure times and different temperatures. Dark measurements will be obtained during each calibration procedure. This way information is obtained on the stability of the detector noise and the dark signal throughout the calibration measurement period.

4.4. Description of the In-flight measurements

In-flight calibration is performed based both on dedicated measurements and on routine radiance and irradiance measurements. For the dedicated measurements the OMI has two types of light sources on-board: the White Light Source (WLS) and the Light Emitting Diodes (LEDs). In addition, specific dark current measurements are also performed. In Table 4.3 it is shown which in-flight measurements are used for the calibration of which parameter. More details about the precise procedures followed can be found in the *Instrument operations and in-flight calibration and monitoring* [RD-3]. Each measurement includes a read-out of the empty register, which yields the electronic offset for the four amplifier gain settings and a determination of the read-out noise.

Table 4.3: List of in-flight calibration measurements and the quantities listed in the OPF that they provide.

Measurement	Quantity
LED	Dead pixel map, relative electronic gain values
WLS	Dead pixel map, PRNU, non-linearity checks, CTE maps, relative electronic gain values
Dark	Dark current, dead pixel map, CTE maps, offset map, relative electronic gain values
Sun	Wavelength calibration, BRDF
Earth	Wavelength calibration

4.4.1. Earth radiance measurements

Earth radiance measurements will be used to obtain wavelength calibration parameters, to be stored in the Level 1B calibration product. Based on these measurements the calibration scientist will be able to monitor the wavelength calibration of the instrument and eventually update the parameter values in the OPF.

4.4.2. Sun irradiance measurements

The sun irradiance measurements will be used both for normalising the earth measurements and for monitoring the radiometric response of the instrument, including the BRDF. The latter is done by using three different reflectance diffusers, as described in the second chapter of this ATBD. Just as for the Earth radiance measurements, wavelength calibration is performed and values in OPF are regularly updated.

4.4.3. LED measurements

The LEDs are placed very close to the detectors and therefore illuminate the entire section of the CCD that is not covered. This includes both the areas that are illuminated by the radiance and irradiance measurements as well as the stray light rows. Its main purpose will be the monitoring of bad pixels. In view of the near monochromatic nature of the light it emits, it is less suited for the determination of the pixel response non-uniformity (PRNU), though it may be used in conjunction with the WLS measurements. LED measurements can also be used to obtain relative electronic gain values.

4.4.4. WLS measurements

The white light source (WLS) illuminates the same area on the CCD as the radiance and irradiance measurements, as it fully illuminates the spectrograph slit. This ensures that each CCD pixel will be illuminated by light of the same wavelength as for the radiance and irradiance observations. This enables monitoring of the PRNUs of the illuminated CCD pixels. If needed, the WLS may also be used for checks on the linearity behaviour of the instrument. However, this requires special measurements and is not expected to be part of routine operations. Furthermore, CTE effects and relative electronic gain values can be monitored.

4.4.5. Dark current measurements

During each measurement there is a build-up of dark current electrons. This build-up must be characterised accurately if it is to be removed from the measurement. Measurements of the dark current can be performed both on the dark side of the orbit, as well as on the dayside. Furthermore, each routine radiance and irradiance measurement will contain information about the dark current, through the non-illuminated rows and columns of the CCD. In order to facilitate and optimise the subtraction of the dark signal, the dark current will be measured with the exact same instrument settings as all the other measurements from which the dark current should be subtracted. In addition long exposure dark current measurements will be done, to obtain dark current maps of the CCD for both the image and the storage region. These measurements are also used to monitor CTE effects, offset values, relative electronic gain values, and the dead pixel map.

4.5. Reference Documents

RD-1. Calibration Plan, *PL-OMIE-0000-TPD-127*, issue 3, February 2001
RD-2. Algorithm Theoretical Basis Document for Level 0 to 1B processing, *RP-OMIE-0000-FS-146*, issue 3, May 2001
RD-3. Instrument operations and in-flight calibration and monitoring, PL-OMIE-KNMI-278, issue draft, May 2001

5. OMI Operations

P.F. Levelt[1], G.H.J. van den Oord[1], J.P. Veefkind[1], and M.R. Dobber[1]
[1]Royal Netherlands Meteorological Institute (KNMI), De Bilt, The Netherlands

This chapter presents a high-level overview of the instrument operations of OMI. Instrument operations concern the activities needed for the commanding of the instrument and safeguarding its health. In the operations of OMI, teams are involved from The Netherlands (KNMI) and the U.S.A. (NASA). The tasks and responsibilities of these teams are discussed section 5.1. From the point-of-view of operations, there are two important phases in the lifetime of OMI: the Launch and Early Orbit operations (LEO) phase and the Nominal Operations phase. These phases are discussed in sections 5.2 and 5.3, respectively. For certain special events, for example in case of a volcanic eruption or during a (validation) measurement campaign, off-nominal operations with special instrument configurations may be required. Operational procedures related to these special events are discussed in section 5.4.

5.1. Responsible entities, communication links and activities

The responsibility for the commanding of the OMI instrument resides with the Flight Operation Team (FOT), at NASA GSFC, and the Instrument Operation Team (IOT), at KNMI. The FOT will be responsible for the functioning of the spacecraft, the communication with the spacecraft and its instruments, and for handling spacecraft and instrument anomalies. The IOT, situated in The Netherlands, is responsible for scheduling daily operations of OMI, preparing the command file (Master Command Load or MCL) and for health and safety monitoring of the OMI instrument. The latter includes trend monitoring of instrument parameters based on engineering and house keeping data. The IOT is also involved in solving the instrument anomalies that may occur during the lifetime of the mission.

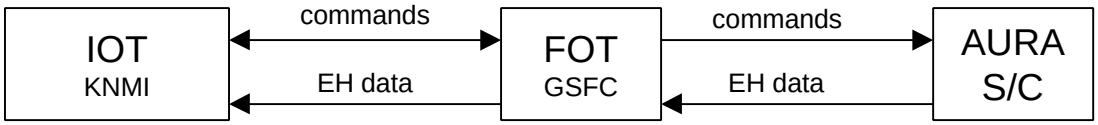

Figure 5.1 Communications between the IOT, FOT and the Aura Spacecraft.

The high-level communication flow between the IOT, FOT, and the spacecraft are illustrated in Figure 5.1. The command file (MCL) that is generated by the IOT in The Netherlands is send to the FOT. After the MCL is checked several times between the IOT and FOT, it is uplinked to the spacecraft by the FOT. The engineering and housekeeping (EH) data are sent back from the spacecraft to the FOT, and from the FOT to the IOT. These engineering and housekeeping data are used for trend monitoring of instrument parameters. The IOT interacts primarily with the FOT through the Instrument Support Terminal (IST). During OMI operations there will also be a passive IST located in Finland. This will permit the Finnish partner to have access to the housekeeping data and mission operations information in order to assist with anomaly resolution involving the Finnish hardware, and to plan Direct Broadcast contacts with the spacecraft. The engineering parameters of the IAM will be monitored in the U.S.A.

Occasionally the IOT may be involved in real-time operations, when required.

Until the nominal operations start the Instrument Planning Group (IPG) represents the IOT at the FOT.

The interactions between the FOT and the IOT are described in an Operations Agreement. All information relevant to the operations of OMI will be documented in the Instrument Operations Understanding document (currently under development), which is based on the operations related documents [RD-1 – RD-4].

5.2. Launch and Early Orbit operations

The Launch and Early Orbit operations (LEO) phase is defined as the period from pre-launch operations to the transition into the nominal operations phase. The pre-launch operations will start 24 hours before the launch. The nominal operations phase will begin approximately three months after the launch of AURA. During the LEO phase the spacecraft and the instruments are subject to several tests. These involve functional tests and the instrument (in-flight) calibration activities.

During the LEO phase, the OMI IOT will be situated at NASA GSFC, to keep communications lines with the FOT as short as possible. A close cooperation between Fokker Space, TRW, NASA, Litton and the OMI Science team is anticipated. The responsibilities for the LEO phase will be shared between those parties.

5.3. The Nominal Operations Phase

The Nominal Operations phase will start approximately three months after launch and will continue until the de-activation operations start. During the Nominal Operations phase, the IOT will be located at KNMI in The Netherlands. The IOT is responsible for the nominal operations of OMI, together with the FOT. The main activities of the IOT will be to schedule the various orbital activities and to generate the MCL. A second main task of the IOT involves trending of instrument parameters from the engineering and housekeeping data, and monitoring the health and safety of the instrument. The FOT activities include uploading the commands to the spacecraft, monitoring the health of the Aura spacecraft, and taking care of urgent mission-threatening events concerning the instrument. Furthermore, the IOT and FOT work together to perform real-time operations (if needed) and to translate Principal Investigator requests into operational activities.

Currently the OMI team is working on definitions of the nominal orbits. These nominal orbits basically consist of Earth observations at the day-side of the orbit, and calibration measurements at the day- and night-side of the orbit. The signal detected by OMI will, apart from factors like clouds and surface albedo, mainly be determined by the solar zenith angle. Therefore, the OMI instrument configurations will be a function of orbital phase. Along an orbit various instrument settings will be changed to optimize the measurements for the changing solar zenith angle. Each instrument configuration can be considered as an orbital activity. These activities are scheduled with respect to the sub-solar point crossing or the terminator crossing. Because the solar zenith angle is the driving factor, OMI operations will be independent of season. An exception to this rule is that the presence of the ozone hole requires special optimized instrument settings during part of the year.

The basic observational modes for Earth observations are the Global, Spectral zoom-in, and Spatial zoom-in modes, as discussed in chapter 2. Most of the time OMI will measure using the Global Mode. A possibility exists to use the Spatial zoom-in mode as the default at high latitudes. At these latitudes, daily global coverage can be obtained using the 725 km swath of the Spatial zoom-in mode. Whether this will become the default at high latitudes is still to be decided by the International OMI Science Team.

To ensure data quality of the Level 1B data product of OMI numerous calibration measurements are scheduled. These calibration measurements are discussed in chapter 4 and include Sun observations, dark current measurements, WLS and LED measurements, and geolocation calibration measurements. These calibration measurements are scheduled in such a way that they permit to monitor and trend all relevant parameters contained in the Operational Parameter File (see chapters 3 and 4).

A fundamental choice for OMI operations is to have these operations as stable and predictable as possible. Above, it was already noted that OMI operations will be based on orbital phase and, consequently, will be independent of season. A second choice is to base operations also on the orbital repeat cycle of the EOS-Aura spacecraft. This repeat cycle is about 16 days (233 orbits). Therefore, an 'OMI-month' has been defined that corresponds to two orbital repeat cycles (466 orbits or about 32 days). This implies that going from one 'OMI-month' to the other, all measurements are repeated at the same relative position, which has advantages for trend monitoring. This resulted in the following definitions:

- an 'OMI-day' consists of 14 nominal (N) orbits and one so-called daily (D) orbit.
- an 'OMI-week' consists of 7 'OMI-days' and 3 special orbits, called weekly orbits (W1,W2,W3).
- an 'OMI-month' consists of 4 'OMI-weeks', and a number of *leap orbits* to fill up the 466 orbits of the orbital repeat cycle. The set of *leap orbits* consists of two 'OMI days', two nominal orbits and two special orbits, called monthly orbits (M1, M2).

During the nominal orbit, measurements in the global and possibly zoom-in modes will be taken at the day-side of the orbit. At the night-side several dark-current measurements will be taken. These nominal orbit measurements will be repeated during the daily, weekly and one of the monthly orbits. During the daily, weekly and monthly orbits also extra activities will be scheduled. In the daily orbit, a LED measurement and a Sun observation will be taken with the daily volume diffuser. The weekly orbits serve as orbits where a Sun observation is done with the first back-up diffuser, a Sun observation is done with the daily volume diffuser using different CCD-settings and a WLS measurements will be taken. During one of the monthly orbits, the second backup diffuser will be used in the Sun observation and WLS and LED measurements will be taken. The second monthly orbit will be used for only dark current measurements, in this case also at the day-side of the orbit.

As an example, in Figure 5.2 the daily orbit is shown, illustrating some of the activities performed during the orbit. In Table 5.1 the sequence of orbits during an OMI-month is shown. The advantage of this scheme is that only five times per month the IOT has to schedule special activities in the command load to the FOT that differ from the daily command load. Consequently, the OMI-SIPS will be dealing with a special data flow only five times per month.

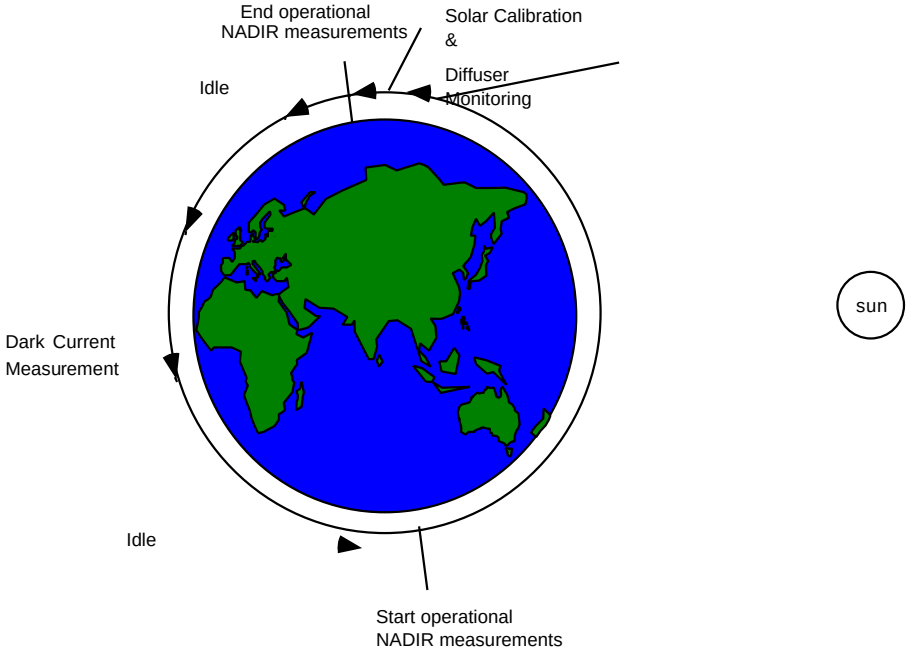

Figure 5.2 The daily orbit for OMI illustrating the scheduling of various orbital activities.

Table 5.1 Orbits executed during an OMI-month (lasting 466 orbits or two Aura orbital repeat cycles). The orbits are executed from left to right and from top to bottom. The Nominal(N), Daily (D), Weekly (W1, W2, W3) and Monthly (M1, M2) orbits all contain different activities. An OMI-month consists of four OMI weeks and a number of so-called leap-orbits. This orbital scenario will be executed approximately sixty times during the lifetime of OMI. The different types of orbits are constructed in such a way that continuing from one type into another goes without interruptions.

N	N	N	N	N	N	N	N	N	N	N	N	N	N	D				1
N	N	N	N	N	N	N	N	N	N	N	N	N	N	D				2
N	N	N	N	N	N	N	N	N	N	N	N	N	N	D				3
N	N	N	N	N	N	N	N	N	N	N	N	N	N	D				4
N	N	N	N	N	N	N	N	N	N	N	N	N	N	D				5
N	N	N	N	N	N	N	N	N	N	N	N	N	N	D				6
N	N	N	N	N	N	N	N	N	N	N	N	N	N	D	W1	W2	W3	7
N	N	N	N	N	N	N	N	N	N	N	N	N	N	D				8
N	N	N	N	N	N	N	N	N	N	N	N	N	N	D				9
N	N	N	N	N	N	N	N	N	N	N	N	N	N	D				10
N	N	N	N	N	N	N	N	N	N	N	N	N	N	D				11
N	N	N	N	N	N	N	N	N	N	N	N	N	N	D				12
N	N	N	N	N	N	N	N	N	N	N	N	N	N	D				13
N	N	N	N	N	N	N	N	N	N	N	N	N	N	D	W1	W2	W3	14
N	N	N	N	N	N	N	N	N	N	N	N	N	N	D				15
N	N	N	N	N	N	N	N	N	N	N	N	N	N	D				16
N	N	N	N	N	N	N	N	N	N	N	N	N	N	D				17
N	N	N	N	N	N	N	N	N	N	N	N	N	N	D				18
N	N	N	N	N	N	N	N	N	N	N	N	N	N	D				19
N	N	N	N	N	N	N	N	N	N	N	N	N	N	D				20
N	N	N	N	N	N	N	N	N	N	N	N	N	N	D	W1	W2	W3	21
N	N	N	N	N	N	N	N	N	N	N	N	N	N	D				22
N	N	N	N	N	N	N	N	N	N	N	N	N	N	D				23
N	N	N	N	N	N	N	N	N	N	N	N	N	N	D				24
N	N	N	N	N	N	N	N	N	N	N	N	N	N	D				25
N	N	N	N	N	N	N	N	N	N	N	N	N	N	D				26
N	N	N	N	N	N	N	N	N	N	N	N	N	N	D				27
N	N	N	N	N	N	N	N	N	N	N	N	N	N	D	W1	W2	W3	28
N	N	N	N	N	N	N	N	N	N	N	N	N	N	D				29
N	N	N	N	N	N	N	N	N	N	N	N	N	N	D	N	N	M1	M2	30
1	2	3	4	5	6	7	8	9	10	11	12	13	14	15	16	17	18	19	

5.4. Special Events

For certain special events, a different instrument configuration may be needed. Examples of such events are volcanic eruptions, ozone hole conditions and field campaigns. Some of these events may be known well in advance, like a field campaign or an extended calibration period, while others cannot be foreseen, such as an eruption of a volcano or the occurrence of an ozone mini-hole.

Requests for a special OMI measurement should be send to the IOT. The IOT will check if a request interferes with other OMI operations. In case of conflicting interests of different OMI investigators, the IOT will ask the OMI Science Advisory Board (OSAB) for a decision. For certain special events, like the volcanic eruption, there may not be the time to wait for an OSAB decision. In this case the IOT will ask the OMI PI for a decision. If nor the PI, nor any member of OSAB can be reached in time, the IOT will decide if a request will be granted. The OMI investigators will be informed on all off-nominal operations as soon as these are scheduled.

5.5. Reference Documents

RD-1. OMI Operation Concept, *RP-OMIE-0000-FS-145*, issue 1, December 2000
RD-2. OMI Instrument Operations Manual, *RP-OMIE-0000-FS-329*, issue draft, December 2000
RD-3. OMI Launch and Early Operations Handbook, *RP-OMIE-0000-FS-330*, issue draft, December 2000
RD-4. Input for timeline development, *RP-OMIE-KNMI-289*, issue draft, August 2001

6. Acknowledgements

The authors of this ATBD specially thank Johan de Haan (KNMI) for his valuable comments and suggestions on earlier versions of this ATBD. They also thank Ernie Hilsenrath (NASA-GSFC) and Gilbert Leppelmeier (FMI) for their comments.